This is to certify that the

thesis entitled

Laser Surface Modification of Titanium Aluminides to Improve Oxidation Resistance at Elevated Temperatures

presented by

Yong Wook Sin

has been accepted towards fulfillment
of the requirements for

Master's degree in Materials Science

Dr. N. Subramanian

Major professor

Date 2/21/90

LASER SURFACE MODIFICATION OF TITANIUM ALUMINIDES TO IMPROVE OXIDATION RESISTANCE AT ELEVATED TEMPERATURES

By

YONG WOOK SIN

A THESIS

Submitted to

MICHIGAN STATE UNIVERSITY

in partial fulfillment of the requirements

for the degree of

MASTER OF SCIENCE

Department of Metallurgy, Mechanics and Materials Science

1990

ABSTRACT

LASER SURFACE MODIFICATION OF TITANIUM ALUMINIDES TO IMPROVE OXIDATION RESISTANCE AT ELEVATED TEMPERATURES

By

Yong Wook Sin

Ti_3Al has low density and good mechanical strength at high temperature. But it also has major drawbacks such as low temperature brittleness and poor oxidation resistance at elevated temperatures.

The maximum use temperature of this material depends on the improvement of oxidation resistance rather than that of mechanical properties such as creep or strength.

Al_3Ti has very good high temperature resistance because of its high contents of aluminum present. High aluminum contents makes protective Al_2O_3 layer on the surface of the material.

In this study, Al_3Ti coating on to the surface of Ti_3Al was formed by using laser surface modification technique. The effectiveness of coating was investigated before and after 10 hours cyclic oxidation process.

To My Father, Mother and Wife

ACKNOWLEDGEMENT

I wish to express my greatest appreciation to my advisor, Dr. K.N. Subramanian for his patient guidance and enthusiasm in every aspect of this research, his friendship and frequent encouragement throughout my studies.

I would like to thank Dr. Mukherjee for allowing me to use laser facility and Dr. Grummon and Dr. Crimp for their kind guidence. I also would like to thank Mr. Donald E. Larson Jr. of Howmet corporation, whitehall, MI for kindly providing me Ti_3Al and Al_3Ti samples used in this study. Special thanks are also due to Dr. Khan and Mr. Shull for his kind help to use the laser and WDS respectively.

I also would like to express my deepest gratitute to my parents for their endless love, encouragement and supports. The last but not the least, I would like to thank to my wife, *Hae-Jeong*. Without her endurence,sacrifice and encouragement to me, the accomplishment of my studies may not be possible.

Feburary 19, 1990

TABLE OF CONTNETS

LIST OF FIGURES

LIST OF TABLES

1. INTRODUCTION

1-1. INTRODUCTION AND HISTORICAL BACKGROUND

Realization of the hypersonic aerospace vehicle for the 21st century depends on the development of advanced high temperature materials for its high temperature gas turbine engine. The development of titanium alloys for different jet engine parts (fan, high compressor blades and disks) has been carried out for 40 years after the gas turbine rotor was made of titanium alloys for the first time in 1950's [1-4]. Titanium alloys have substituted nickel-based and iron-based superalloys because of their low density and comparable strength [5].

Since then, titanium alloys have been improved considerably and they can reach higher tensile strength at relatively low temperatures (20 - 430°C). They also have good creep strength for temperature up to 600°C [6]. Titanium alloys, however, have some inherent limitations such as low creep strength and poor oxidation resistance properties above about 650°C [7].

The need for high performance aircraft has been increased in the last decade. Hence, the development of new materials for high performance gas turbine engine has been

necessitated. Among the available intermetallics, titanium aluminides (Ti_3Al and TiAl) have received significant attention as potential structural components because they have low density and relatively high strength at elevated temperatures. But both of these intermetallics (Ti_3Al and TiAl) possess poor high temperature oxidation resistance, and are brittle at the room temperature [1,5,8,9-23]. The oxidation resistance of Ti_3Al is worse than that of TiAl [5]. This phenomenon is attributed to the inability of the aluminum present in these intermetallics to provide a protective oxide layer on their surfaces [24].

Because of aforementioned reasons, extensive studies on the development of titanium aluminides as potential structural materials for high temperature applications have been carried out.

Titanium alumnides have ordered structures (superlattices), and are composed of a simple ratio of titanium aluminum (A_XB_Y where X and Y are integers) [25]. In the free energy curve, they have a very narrow stability range which causes a rapid rise in G (Gibb's free energy) with small composition fluctuations [26]. Titanium aluminides (intermetallics) have superlattices (Ti_3Al has DO_{19}, TiAl has $L1_0$ and Al_3Ti has DO_{22}) [8,24,27,28]. The comparisons of crytal structures, lattice parpmeters and thermal expansion coefficients of Ti_3Al and Al_3Ti are

illustrated in Table 1. These materials have good high temperature properties because of the strong A-B bond and high activation energy. But this strong A-B bond results in low temperature brittleness [25,26].

Enhancement of the low temperature ductility of these intermetallics can be achieved by alloying additions [5,9-11,29]. For example, Blackburn, et al. improved the low temperature ductility by using niobium alloying additions in Ti-Al system (Ti-16Al-10Nb) [29]. Joseph et al. found that the mechanical properties of niobium alloyed titanium aluminides decreased at elevated temperatures because of embrittlement by oxidation [30].

On the other hand, another intermetallic present in the Ti-Al system, namely Al_3Ti was found to have very good high temperature oxidation resistance [24,31]. Higher contents of aluminum present in this intermetallic can facilitate the formation of a protective Al_2O_3 oxide layer [24,32]. In 1985, Stoloff [33] reported that Al_2O_3 layer, although brittle, is formed on the aluminide surface as in the case of NiAl, protecting the NiAl substrate from the oxidation up to 1000°C. In the case of Kanthal, an iron-aluminum alloy, similar of Al_2O_3 layer is formed on the surface of substrate to give a good oxidation resistance up to about 1600°C. Kanthal has been used as heating elements for quite same time [23,33].

Table 1. The comparisons of crystal structure, lattice parameters and thermal expansion coefficients of Ti_3Al and Al_3Ti.

Materials	Crystal structure	Lattice parameter			Thermal expansion coefficient	
		a A°	c A°	c/a	along a $(°K)^{-1}$ $(x10^6)$	along c $(°K)^{-1}$ $(x10^6)$
Ti_3Al	DO_{19}	5.765	4.625	0.80225	12.86 (900°K) 8.29 (300°K)	13.26 (900°K) 9.04 (300°K)
Al_3Ti	DO_{22}	3.85	8.596	2.234		

Lipsitt also suggested that coatings could improve the high temperature oxidation resistance of titanium aluminides [24,25,34]. In 1987, Yamaguchi [24] reported that Al_3Ti, unlike Ti_3Al and TiAl, forms only Al_2O_3 layer on the surface which protects the substrate from oxidation. He also suggested that Al_3Ti can be used for coating materials to protect Ti_3Al and TiAl as well as Titanium from the high temperature oxidation. Problems relating to its room temperature brittleness have also been encountered in Al_3Ti.

Extensive studies have been carried out to overcome the two major drawbacks, of low temperature brittleness and poor oxidation resistance in high temperature applications [30,35-45].

Firstly, the poor oxidation resistance at high temperatures can be improved by alloying. Chromium and vanadium additions to the Ti-Al system form alumina scales on the surface of materials in the air at 1100-1400°C. Ti-30Al-12Cr-15V alloy forms a single layer of alumina scale in the air at 1400°C [2]. These alumina scales protect the materials from high temperature oxidation. But the addition of these rare-earth elements decreases the melting point of materials, resulting in degradation of mechanical properties at high temperatures. Hence, the usage of these materials

was restricted to the coating [30]. Several coating processes such as slurry spraying, molten dipping and pack cementation have been used for several decades [46]. However, laser surface modification which is used widely because of its convenience and effectiveness in several systems, has not be applied to titanium aluminides.

Secondly, low temperature brittleness has been improved by using several following methods:

Alloy chemistry modification

The addition of vanadium, chromium and manganese to the titanium aluminides improves the ductility, decreasing the volume of the unit cell so as to form strong chemical bonding [5]. On the other hand, the addition of niobium and tungsten decreases the ductility, although it increases the strength.

Improved fabrication process

Improved processing techniques such as PM/RS (Powder metallurgy / Rapid solidification) method improves the high temperature strength and ductility as a result of diminishing grain size [2,47].

Microstuctural features

(1) The increase of ductile alloy composition (γ-phase only with 47-49 at.% aluminum content) in the two-phase ($\alpha_2+\gamma$) region in TiAl was proposed to improve ductility by Kim [5].
(2) Precipitation of a ductile second-βphase (bcc structure) in Ti_3Al + Nb + W alloys improves ductility [12].
(3) The improvement of ductility by addition of vanadium, chromium or manganese to the TiAl is attributed to twinning. Niobium addition can reduce the planarity of slip and increase non-basal slip activity, which improves ductility of Ti_3Al [1,5,47].

The present study will focus on Ti_3Al because it is more ductile than TiAl and the mechanical properties of Ti_3Al is improved by adding Niobium, Vanadium and Molybdenum. However, the oxidation resistance of Ti_3Al is still lower than that of TiAl. Al_3Ti coating on Ti_3Al is desirable to improve its high temperature oxidation resistance.

Laser surface modification to achieve the desirable surface properties has received significant attention in recent years [48-53]. The ability to achieve surface modifications without significantly altering the bulk properties of the material is the most important advantage of this technique. Melting of the Al_3Ti onto the surface of

Ti_3Al can be carried out by using lasers. The compatibility of these two intermetallics, and the influence of the Al_3Ti coating on the high temperature oxidation resistance of Ti_3Al will be studied in this project.

The purpose of this study is to retain the structural capabilities of Ti_3Al and at the same time to provide a surface layer of Al_3Ti to improve the oxidation resistance of the system.

1-2. THEORETICAL BACKGROUND

1-2-1. Intermetallics

The formation of ordered phases can be explained with quasi-chemical model of solutions in thermodynamics conveniently.

Assumptions:

(a) The solutions have equal molar volumes in the pure state

(b) No volume change is required when the solutions are mixing together ($\Delta V_m = 0$)

(c) The only nearest neighbor interactions should be considered as the interatomic forces.

Binary solid solution has three types of bonds:

(1) A-A bonds with an E_{AA}

(2) B-B bonds with an E_{BB},

(3) A-B bonds with an E_{AB},

where E_{AA}, E_{BB}, and E_{AB} are the bonding energies of A-A, B-B and A-B bonds respectively.

If P_{AA}, P_{BB} and P_{AB} are the numbers of these three typws of bonds respectively, the internal energy of the solution E_S can be described as follow:

$$E_S = P_{AA}E_{AA} + P_{BB}E_{BB} + P_{AB}E_{AB} \qquad \text{(i)}$$

If n_A atoms of A and n_B atoms of B are in 1 mole of solid solution, and Z is the coordination number of an atom, Then,

$$n_AZ = P_{AB} + 2P_{AA}$$

$$P_{AA} = n_AZ/2 - P_{AB}/2. \qquad \text{(ii)}$$

Similary,

$$P_{BB} = n_BZ/2 - P_{AB}/2. \qquad \text{(iii)}$$

Substituting equations (ii) and (iii) into (i) gives

$$E_S = Zn_AE_{AA}/2 + Zn_BE_{BB} + P_{AB}(E_{AB} - (E_{AA} + E_{BB})/2).$$

On the other hand, energy of the unmixed components are

$$E_{UM} = n_AZE_{AA}/2 + n_BZE_{BB}/2$$

The energy of mixed components are

$$\Delta E_M = P_{AB}(E_{AB} - (E_{AA} + E_{BB})/2).$$

Enthalpy of the mixing process is given by

$$\Delta H_M = \Delta E_M - P\Delta V_M.$$

But $\Delta V_M = 0$.

Therefore,

$$\Delta H_M = \Delta E_M = P_{AB}(E_{AB} - (E_{AA} + E_{BB})/2).$$

In the real solutions, to get a minimum free energy, atoms should be arranged with the lowest internal energy consistent with sufficient ramdomness.

If the value of $E_{AB} - (E_{AA} + E_{BB})/2$ is negative (in a system), the internal energy of the system decreases by increasing

the number of A-B bonds, which results in atomic ordering [26]. For example, in the Cu-Au alloy system, CuAu has the ordered structure which is composed of alternate layers of the Cu and Au atoms at low temperatures. This kind of lattice is called as a superlattice. On the other hand, Cu_3Au has another superlattice. These are illustrated in Fig. 1 [26].

Titanium aluminides (Intermetallics) also have ordered structure (superlattice) like Cu-Au alloy system.
The binary system of Ti-Al phase diagram is shown in Fig. 2 [47]. The phase diagram of titanium-aluminum system indicates that there are four phases such as high temperature disordered α-Ti, disordered β-Ti, ordered hexagonal α_2-Ti_3Al and ordered face-centered tetragonal γ-TiAl [5].

Figure 1. Ordered substitutional structures in the Cu-Au system: (a) CuAu superlattice. (b) Cu_3Au superlattice [26].

Figure 2. Binary Ti-Al phase diagram [24].

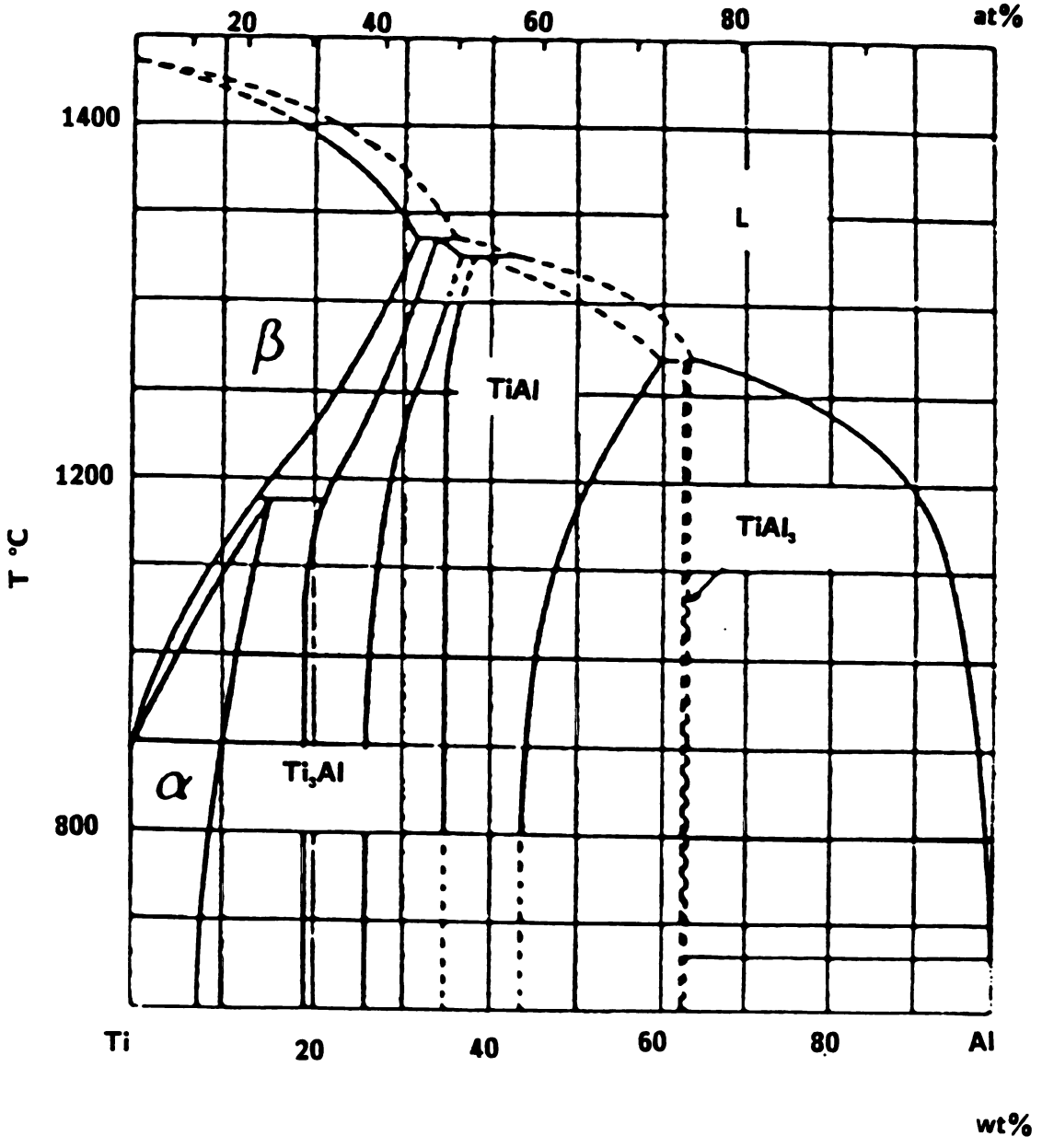
20
40
60
80
at%
1400
1200
800
T °C
L
β
TiAl
TiAl3
α
Ti3Al
Ti
20
40
60
80
Al
wt%

Figure 2.

1-2-2. Laser Surface Modification

In recent years, laser surface modification has emerged as an attractive technique because it is very benificial to modify surface properties without changing bulk properties of materials. Several techniques such as laser-chemical-vapour deposition (LCVD), cladding, alloying, surface hardening and surface melting are included in this category [56].

Laser surface cladding was used in the present study. In cladding, powder is coated on the substrate with a binder and is melted to produce strong bonding with the substrate. (Fig. 3) The beam in this process should be perpendicular (or nearly perpendicular) to the surface of specimen and is mostly defocused. The variables for this process are beam intensity, efficiency, effective heating time and beam diameter. [48]

Figure 3. Laser surface modification (cladding) [26].

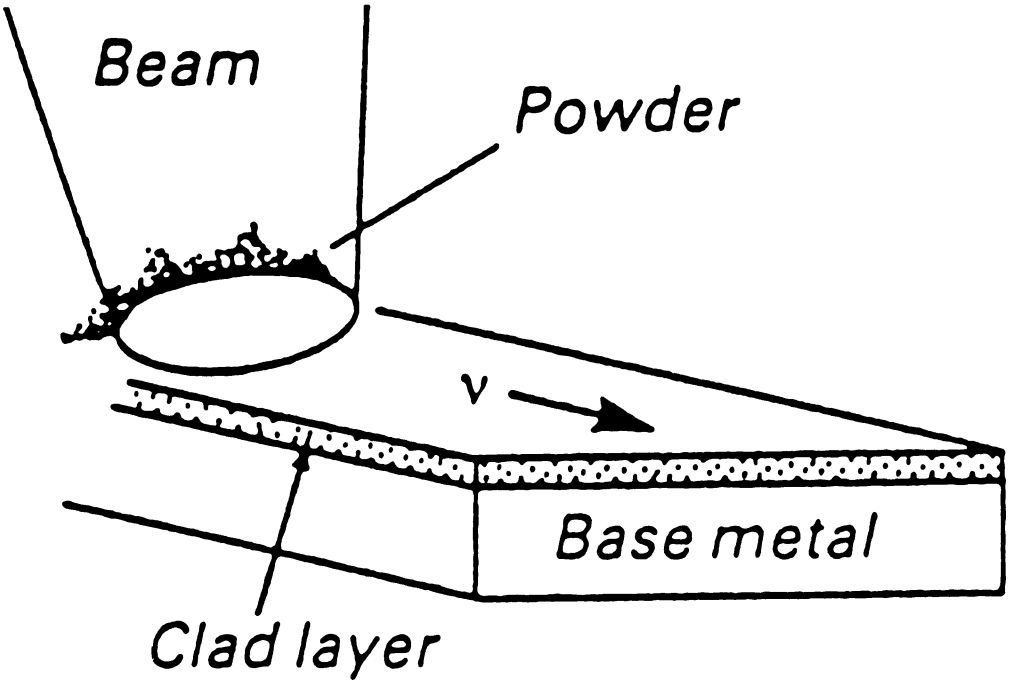

Figure 3.

2. EXPERIMENTAL PROCEDURE

2-1. MATERIALS

Ti_3Al and Al_3Ti intermetallics used in the present study were obtained, in plate and ingot forms respectively, from Howmet Inc. The detailed composition of Ti_3Al is listed in Table 1.

Table 2. The chemical analysis of Ti_3Al stock

Elements	Ti	Al	Mo	Fe	V	Cu	Si	Nb
Wt %	56.3	14	2.07	0.08	3.87	0.15	0.1	23.43
At %	60.8	25	1		3			10

(Ti-25Al-10Nb-3V-1Mo)

2-2. LASER SURFACE MODIFICATION

Among various types of lasers that have been developed for various purposes, usually two types of lasers are used for laser surface modification of metals and ceramics. One such type is solid state laser such as pulsed ruby, and Nd(Neodymium):glass laser; the other type is gas laser such as CO_2 laser. In particular, the application of gas lasers is gaining importance; they have continuous waves, high efficiency (for example, CO_2 laser has around 30 % efficiency), high power and reasonable costs for installation. A 2.0 KW. CO_2 laser was used in the present study.

Ti_3Al and Al_3Ti were prepared for matrix and coating respectively. Small square specimens (10 mm x 10 mm x 3 mm) were cut out from the Ti_3Al plate. The Al_3Ti ingot was crushed and ground to a powder in a ball mill using alumina balls for 24 hours. The Al_3Ti powder was coated on the Ti_3Al plates in the form of slurry prepared with absolute alcohol. The coated specimens were allowed to dry completely for about 20 minutes before laser surface modification.

Several operational parameters need to be considered for laser surface modification process. These include the power of laser, interaction time (beam traveling speed), the range of spot size (beam diameter), and the number of times of remelting. In the present study the beam diameter on the surface of specimen coated by Al_3Ti powder was fixed. Interaction time between the laser beam and specimen, and the number of times of remelting were changed. Helium (He) gas was used as a shielding gas. The shielding gas chamber was specially designed for increasing the efficiency of shielding gas. The gas chamber used in this study is shown in Fig. 4. Surface remelting was carried out along the same track of the same specimen for several times. All laser treatments were accomplished using a defocusd beam. The details of the processing conditions used are listed in Table 2. The graph used for converting the beam diameter to the distance from the nozzle of the laser beam to surface of specimen is given in Fig. 5. The overall features of laser surface modification are illustrated in Fig. 6.

After each laser surface modification process, visual inspection was made and the conditions of beam spot size and traveling speed of the laser beam were changed to find the optimum condition for producing a good coating.

Table 3. The conditions of laser surface modification

The number of times of remelting	1	1	1	2	4
beam speed (in/min)	30	35	40	50	60

* used laser power: 680 W

* used power density: 10^4 J/cm^2

* maximum power density; 10^6 J/cm^2

Figure 4. Shieding gas chamber.

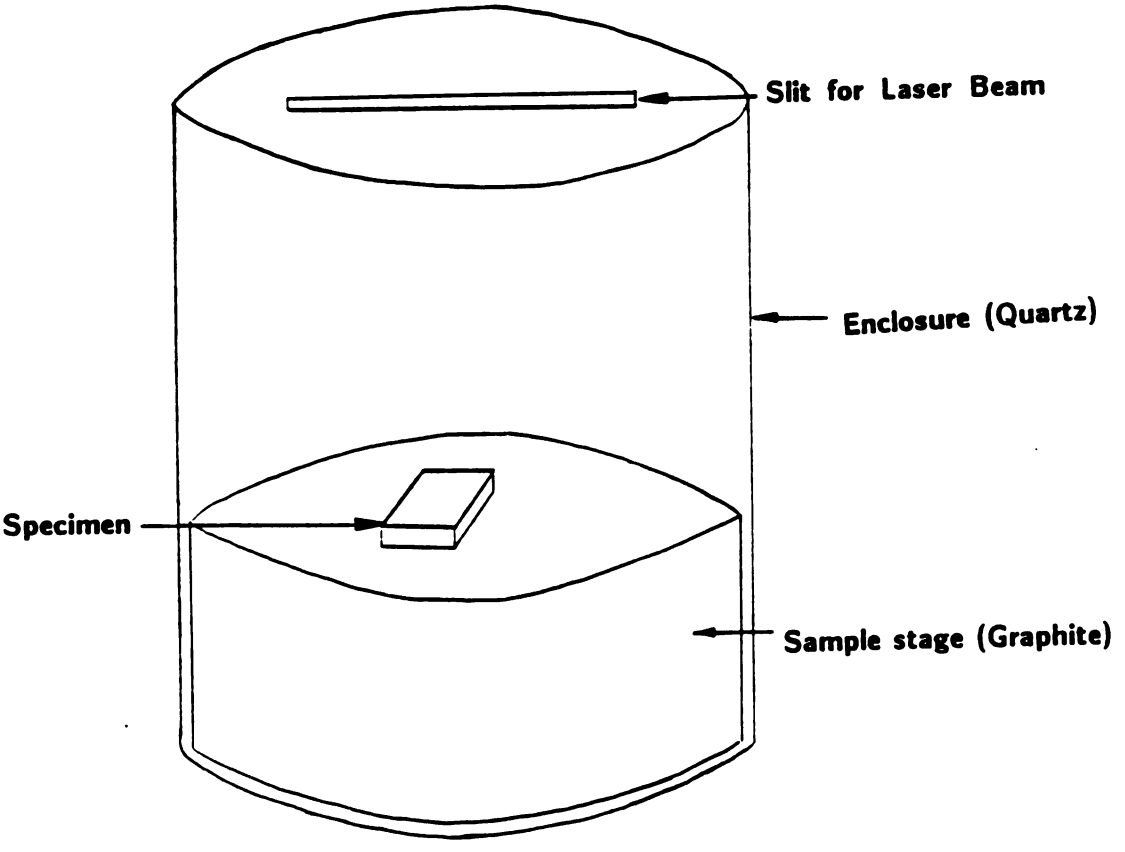
Slit for Laser Beam
Enclosure (Quartz)
Specimen
Sample stage (Graphite)

Figure 4.

Figure 5. Beam focusing chart.

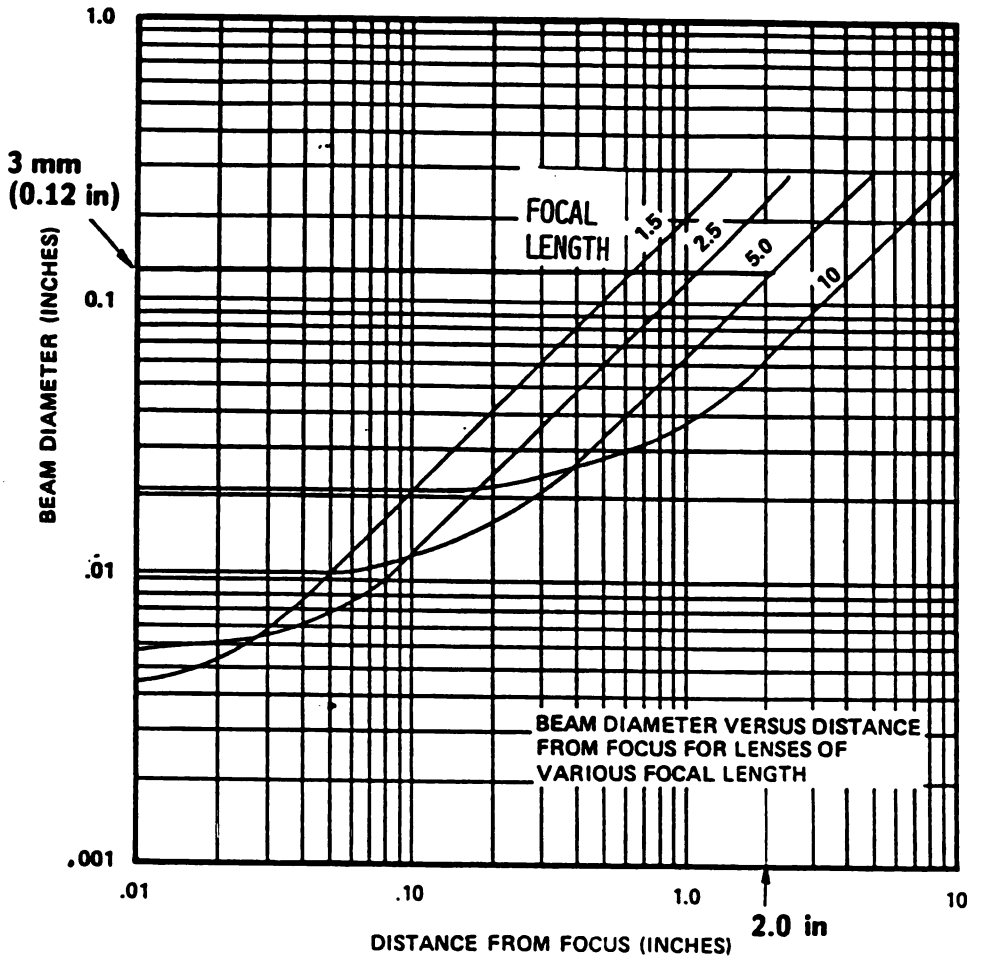
1.0
3 mm
(0.12 in)
0.1
.01
.001
BEAM DIAMETER (INCHES)
FOCAL
LENGTH
1.5
2.5
5.0
10
BEAM DIAMETER VERSUS DISTANCE
FROM FOCUS FOR LENSES OF
VARIOUS FOCAL LENGTH
.01
.10
1.0
10
2.0 in
DISTANCE FROM FOCUS (INCHES)

Figure 5.

Figure 6. Overall features of laser surface modification.

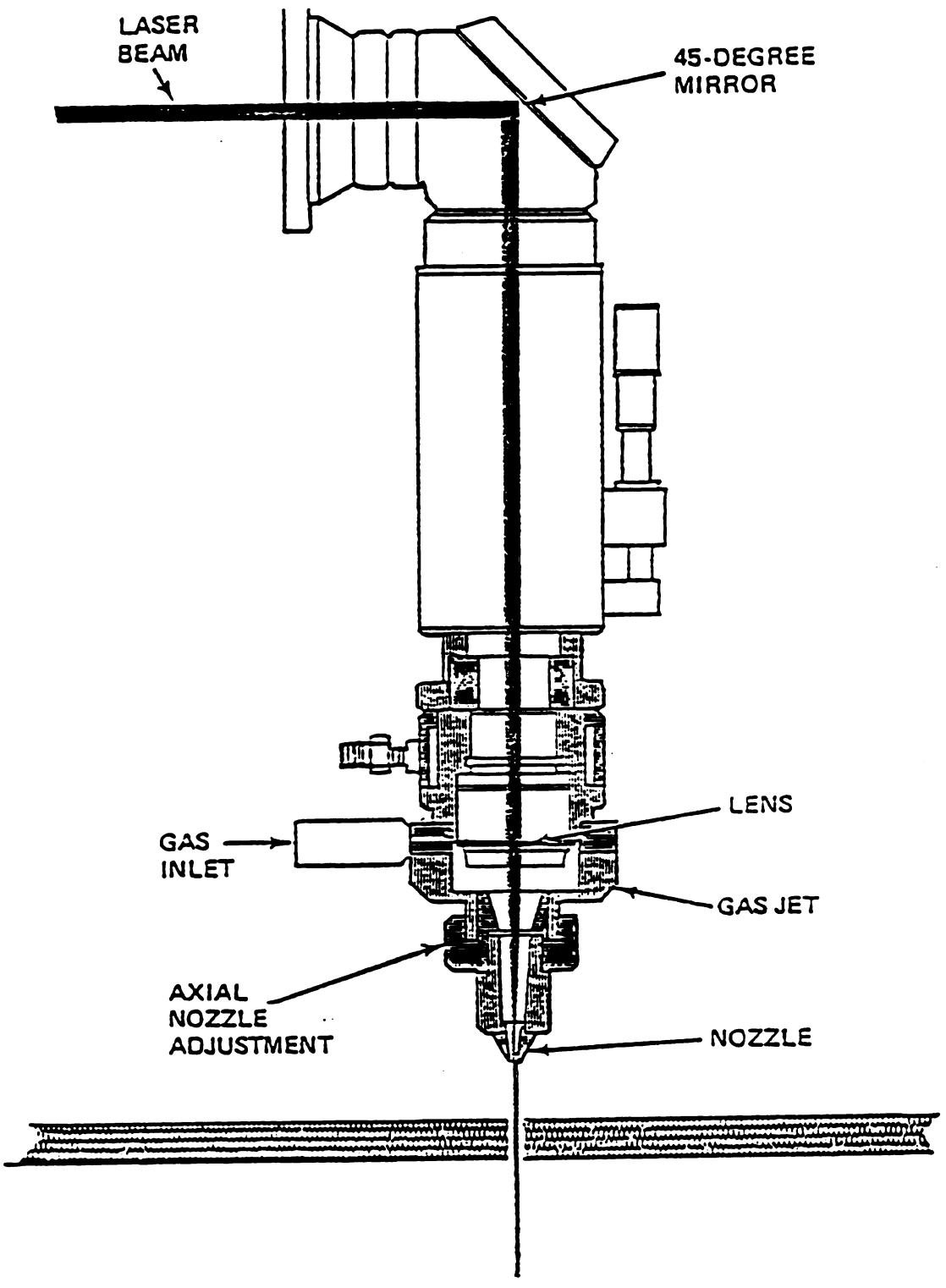
LASER
BEAM
45-DEGREE
MIRROR
LENS
GAS
INLET
GAS JET
AXIAL
NOZZLE
ADJUSTMENT
NOZZLE

Figure 6.

2-3. CYCLIC OXIDATION

Cyclic oxidation was carried out for 10 hours. One cycle of the process consisted of 1 hour of oxidation at 1000°C and 15 minutes of cooling down to ambient temperature.
The specimens treated by the laser were cut in the form of square plates (2.5 mm x 2.5 mm x 3.0 mm) by high speed diamond saw. Cyclic oxidation studies were carried out only on specimens with even coating. The thickness of the coating was almost 1 mm for the specimens selected for oxidation studies. All the selected specimens were polished with sand paper to have even surfaces before cyclic oxidation process.

The oxidized specimens were assessed by several ways. After visual inspection, the oxide formation of coated side and that of uncoated side were investigated by Scanning Electron Microscopy (SEM) and Wavelength Dispersive Spectrometer (WDS).

2-4. SCANNING ELECTRON MICROSCOPY

To determine how Al_3Ti coating protected the Ti_3Al matrix from oxidation, the cyclic oxidized specimens were cut by a diamond saw which is shown in Fig. 7. The cut surface of specimens were ground with # 240 sand paper, followed by # 320, # 400 and # 600 grit papers; they were polished on the rotating wheel with 600 grit, followed by 5 μm, 0.3 μm, 0.05 μm abrasive particles. Interfaces and grain boundaries in specimens were barely seen by naked eye after the polishing procedure. The cross section of the oxidized specimens was investigated by using SEM.

Figure 7. Specimen preparation before and after cyclic oxidation process. (dotted line is indicated cut surface.

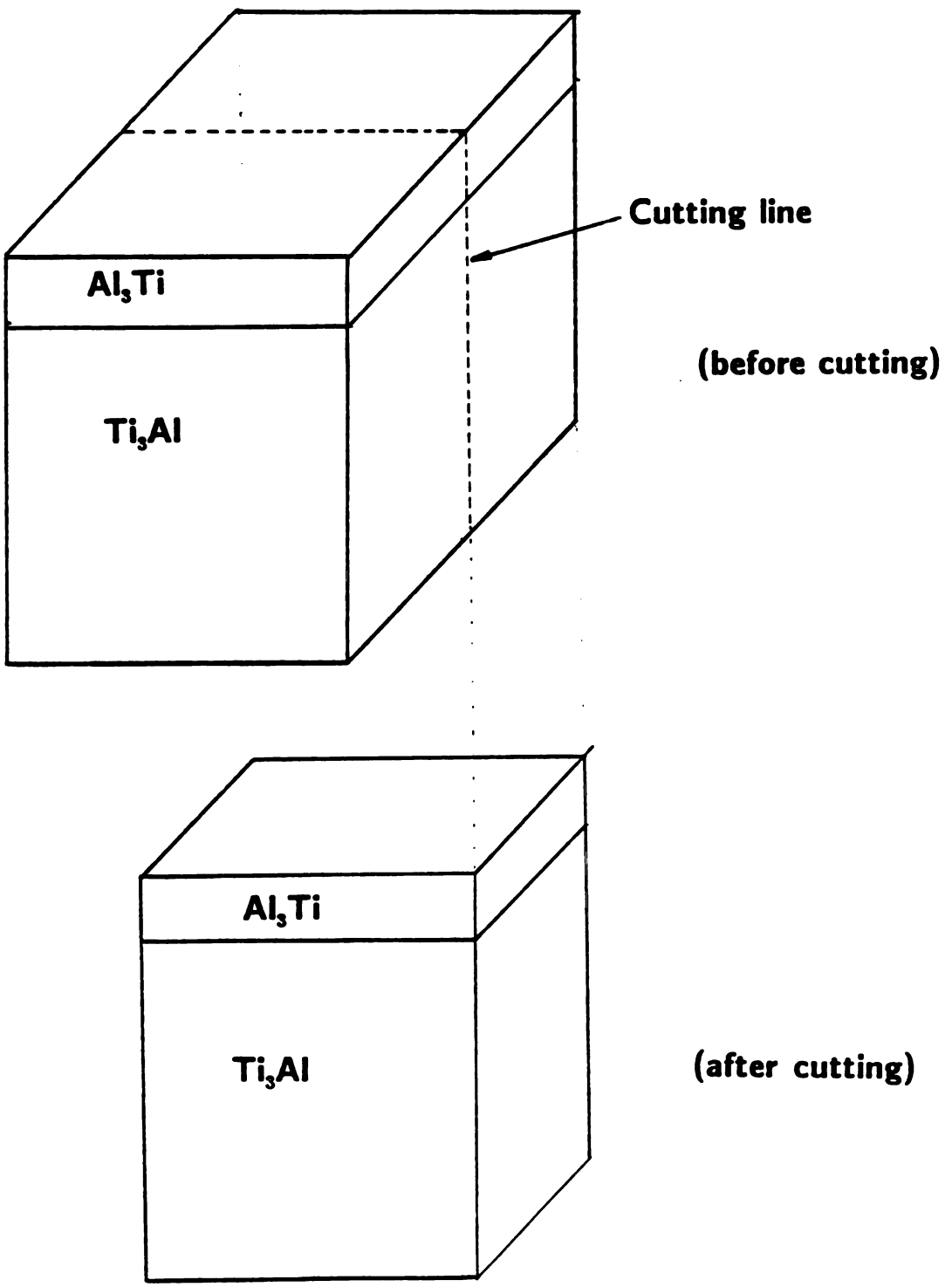
Cutting line
Al_3Ti
Ti_3Al
(before cutting)
Al_3Ti
Ti_3Al
(after cutting)

Figure 7.

2-5. WAVELENGTH DISPERSIVE SPECTROSCOPY

2-5-1. Characteristic X-ray Image

Characteristic X-ray image studies were carried out for determining the concentration profiles of the three major elements such as titanium, aluminum, and oxygen. Sample currents for titanium and aluminum detections were fixed at 0.016 μA (0.03 μA full scale). The amount of oxygen was not enough to be detected on the screen in WDS. So the sample current for oxygen detection was increased up to 0.2 μA (0.3 μA full scale) which was about 12.5 times more than that for titanium and aluminum. Nevertheless oxygen detection based on the image on the screen was still not strong enough. To obtain a sharp image of the oxygen mapping on the screen, the exposure time for oxygen was up to two and a half times longer than that for titanium and aluminum were selected. The exposure time for oxygen was 100 seconds and that for titanium and aluminum were 40 seconds. P 10 (90 % Argon-10 % Methane) gas was used for the X-ray detector for O_2.

2-5-2. Line Scanning

In the characteristic X-ray image study, electron beam swept certain areas on the specimen. In the line scanning, the beam was fixed initially at one point and then beam was scanned along a single straight line on the specimen to record the change in concentration of elements (for example, in the X- and/or Y-direction). The electron beam was kept perpendicular to the specimen surface. The conditions of WDS for line scanning were the same as that for characteristic X-ray image study. The speed of moving beam on the specimen was 0.193 mm / min. The chart speed of recorder was 1 in / min. The line scanning was executed from the top of the coated surface to the bottom end of the matrix (which was negative Y-direction) and from the left side of the uncoated surface to the right side of the uncoated surface (which was positive X-direction). The starting point of the line scanning on the coated surface was at the middle of the full length of the specimen. The starting point of the line scanning on the uncoated side was at the half of the full height of the uncoated portion in which the width of the coating was not included. (Fig. 8) ZAF technique for absorption correction, atomic number correction and fluorescence correction was not carried out in this X-ray analysis.

Figure 8. The starting points and locuses for line scanning.

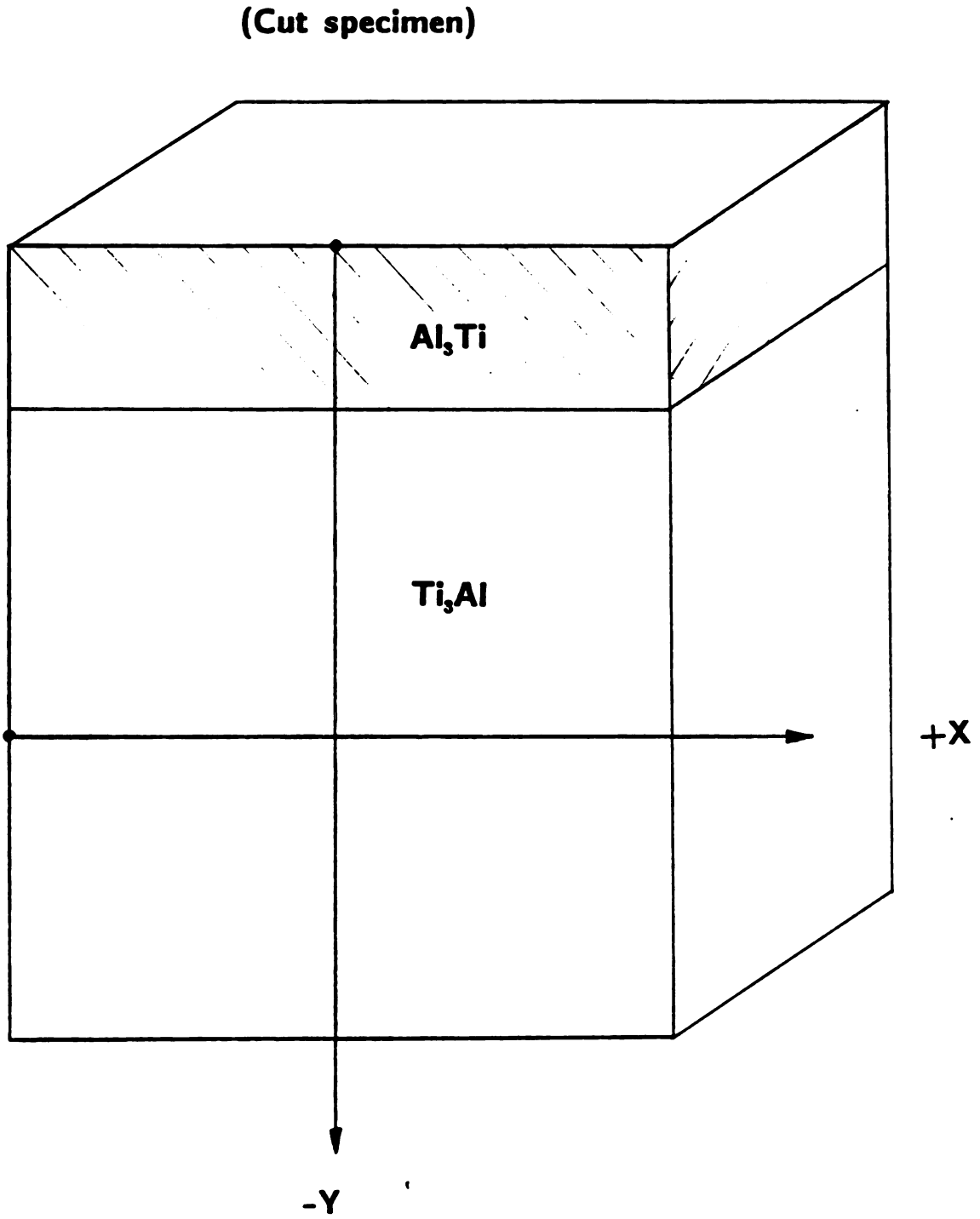

Figure 8.

3. RESULTS AND DISCUSSION

3-1. MICROSTRUCTURAL OBSERVATIONS

The advantages of laser surface coating is that it can provide better specimen surface modification for protection against severe environments without changing the bulk properties. The optimum conditions to produce an even coating of Al_3Ti on the surface of Ti_3Al were obtained by trial and error method. Among the several trials made, five of them yielded specimens suitable for the present study. Although all five specimens had uniform Al_3Ti coatings, two of them exhibited breaks in the coating. The details of laser processing conditions used are already presented in Table 2. The specimens processed by laser with conditions, such as surface remelting speeds of 50 and 60 in/min, and surface melting speed of 35 in/min were selected for investigation by SEM. SEM of these specimens was conducted before and after the cyclic oxidation process. Specimen preparation for SEM studies has been described in the previous chapter.

3-1-1. Laser Surface Treated Specimen

Several kinds of oxide crystals were found on the surface of the coated side, but all these exhibited charateristics of the early stages of oxide formation. The sequence of oxides formed on the coated side depended upon the laser beam speed and the number of times of remelting. Al_2O_3 was formed on the surface of Al_3Ti coating. Continuous oxide crystal layer was formed on the coating when the surface was remelted with a defocused beam at a speed of 50 and 60 in/min. On the other hand, specimens processed by the defocused beam at a speed of 35 in/min formed discontinuous oxide crystal layer (Fig. 9). From the investigations of the microstructure at the interface between the coating and the oxide layer, it was observed that transverse cracks propagated along the interface and new oxides were growing on the Al_3Ti coating at the crack (Fig. 10). It appears that such crack propagation is caused by abrupt temperature change by laser processing. This crack disappeared after cyclic oxidation process, because diffusion between the two phases took place during that process. Such crack can cause decrease the adherence of oxide layer to the coating. The adherence of the coating to the matrix appeared to be very strong, since two components of the system (viz. the matrix and the coating) were mixed well, and there were no

Figure 9. Scanning electron micrographs at the surface of the coated side after laser surface modification: (a) continuous oxide crystals. (b) discontinuous oxide crystals.

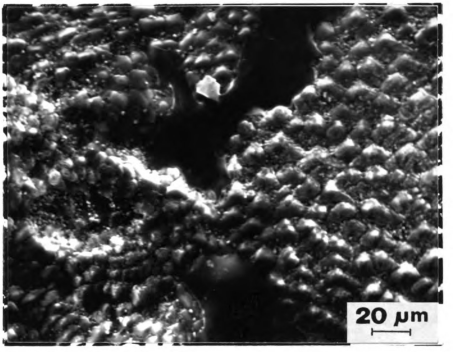

a

Continuous oxide crystals

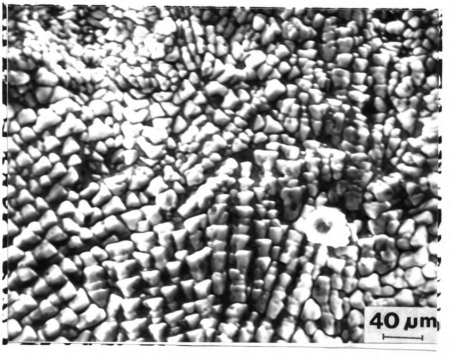

b

Discontinuous oxide crystals

Figure 9.

Figure 10. Scanning electron micrograph of the surface oxide layer after laser surface modification.

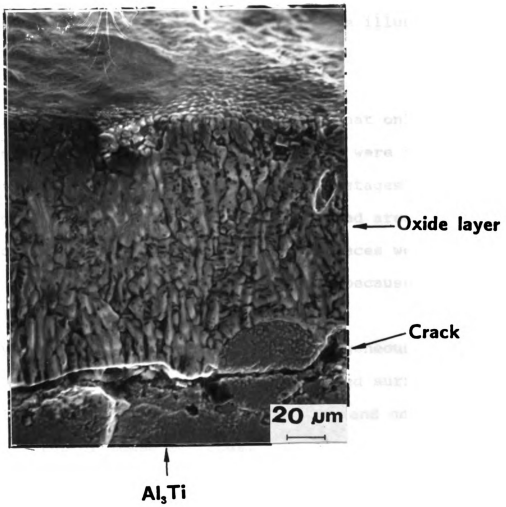

Figure 10.

cracks or pores at the interface. It was also observed that the clear interface line between the coating and the matrix was not fully developed so as to discriminate the two components individually. On the other hand, although grains and grain boundries were formed in the matrix, they could not be observed by SEM. These results are illustrated in Fig. 11.

After laser processing, it was observed that only small areas on the surface of the uncoated side were oxidized. Most of the oxidized areas (in the early stages) were spalled. On the other hand, the unoxidized areas were discolored by the laser beam. These surfaces were not appropriate for cyclic oxidation process because of the following reasons :

Firstly, the specimens did not have homogeneous surface (viz. partly oxidized and spalled surface).

Secondly, melted Al_3Ti coating overflowed and covered the top of these surfaces.

For these resons, these surfaces were not used for oxidation studies. The specimens which had oxide layer only on the surface of the coated side were prepared to study the oxygen penetration profiles at the coated side and at the uncoated side during the cyclic oxidation process.

Figure 11. Scanning electron micrograph of interface between the coating and matrix.

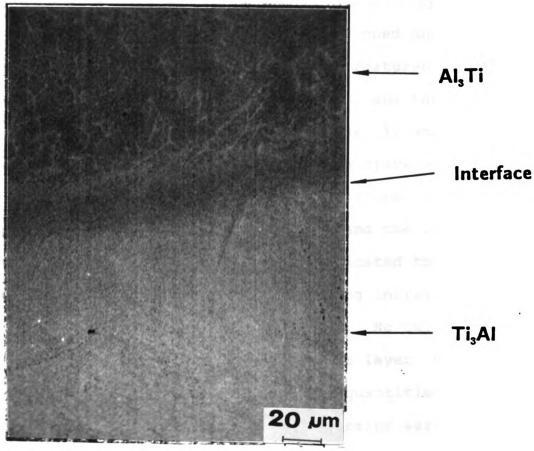

Figure 11.

3-1-2. Cyclic Oxidized Specimen

The specimen used for cyclic oxidation were small rectangular plates cut from the large square Ti_3Al plate. These were coated with Al_3Ti. After 10 hours of cyclic oxidation process, the specimens were sectioned and polished for SEM examination. The microstructural features of the coated side (surface, interface and matrix) and the uncoated side (surface and matrix) are shown in Figs. 12 and 13. It was observed that the oxide layer on the surface of the coated side was more uniform than it was before oxidation process. Cracks between the oxide layer and the coating disappeared. (Fig. 14) These results indicated that the adherence of the oxide layer to the coating increases because of the above mentioned phenomenon. No oxide layers were formed in the coating below the oxide layer, but evidence indicated the presence of small quantities of oxide formation in the subsurface. (Fig. 14) Grains were found in the Al_3Ti coating, even though they were not fully developed at the heat affected zone (HAZ) after cyclic oxidation process (Fig. 14). During the cyclic oxidation process, the surface oxide layer protected the matrix as well as the coating itelf from oxygen penetration.

Figure 12. Scanning electron micrographs at the coated side:

(a) surface.

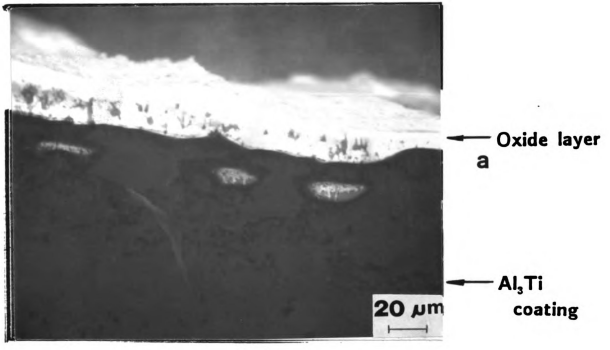

Figure 12.

Figure 12. (continued)

Scanning electron micrographs at the coated side:

(b) interface.

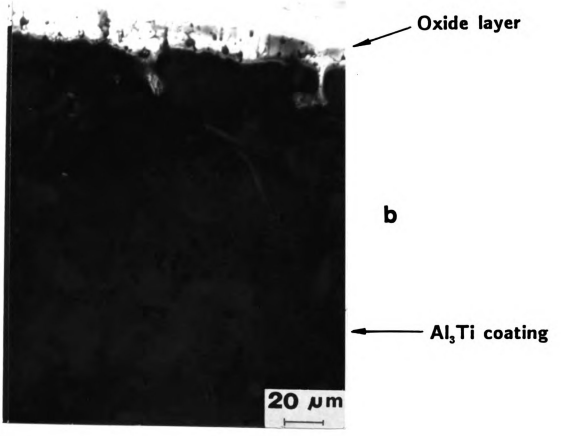

Figure 12. (continued)

Figure 12. (continued)

Scanning electron micrographs at the coated side:

(c) matrix.

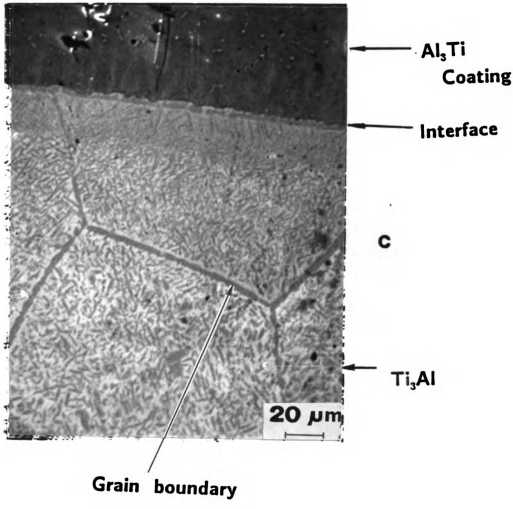

Figure 12. (continued)

Figure 13. Scanning electron micrographs at the uncoated side (surface and matrix).

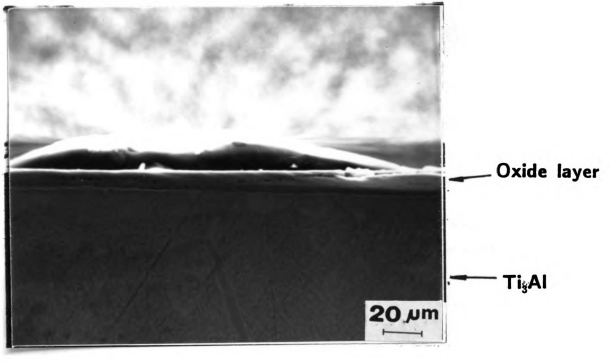

Figure 13.

Figure 14. Scanning electron micrograph of the coating showing the heat affected zone (by laser processing) and the grains.

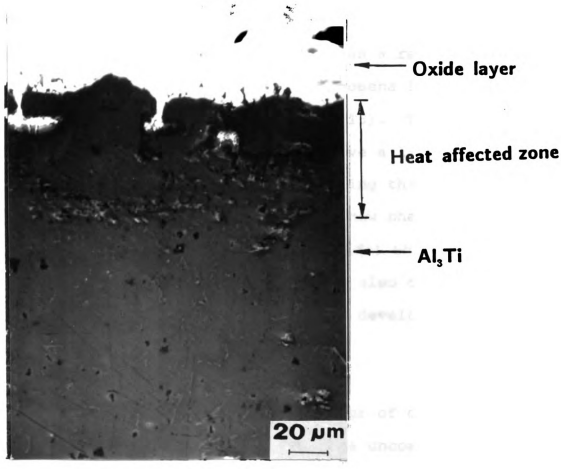

Figure 14.

Tiny pores observed in the coating could be eliminated by using slower laser beam speeds. These results were reported by Oakley et al [57]. After cyclic oxidation, a distinct interface develops between the coating and the matrix. This interface line appears to be very stable as a result of its roughness and interdiffusion. These phenomena led to strong adherence of coating to the matrix (Fig. 15). This diffusion caused the interface line to move a little further into the matrix side, increasing the coating thickness. After 10 hours cyclic oxidation process, new phase was formed near the interface (in the Ti_3Al side) which appears to be probably a TiAl phase [58]. It was also observed that the grains and grain boundaries were well developed in the matrix due to the oxidation treatment.

During the cyclic oxidation process (1 hour of oxidation and 15 minutes of cooling), the surface of the uncoated side was severely oxidized. The morphology and composition of the oxide layer on the uncoated side was totally different from that on the coated side: the latter was Al_2O_3 but the former was TiO_2 (Rutile). The oxide layer formed and spalled during the first cycle of cyclic oxidation process, revealing new surface to air. However, the entire oxide layer did not spall, leaving remnants of the oxide layer on the surface of the uncoated side. This caused the oxide

Figure 15. Scanning electron micrograph of the interface showing strong adherence of coating to the matrix.

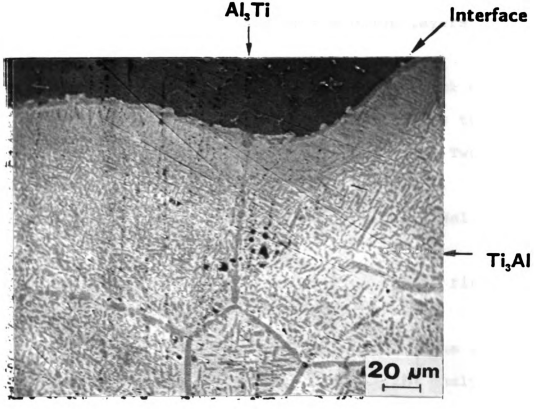

Figure 15.

layers to accumulate, with transverse cracks in-between them. Such results are illustrated in Fig. 16. Two reasons can be used to explain the presence of spalling and transverse cracks after the oxidation process. They are as follows;

(i), the stress and strain of the matrix due to oxidation process are transmitted to the oxide layers [59-61], and

(ii), the stress and strain due to thermal shock during the oxidation process cause the oxide layers to spall.

These two processes occured at the same time. Two models to explain the spalling behavior can be envisaged.

The sequence of steps occuring in the first model are listed below:

(a) the first oxide layer is formed during the first cycle of oxidation process.

(b) the second oxide layer is formed beneath the first layer during the second cycle. Simultaneously, transverse cracks propagated between two layers.

(c) the first oxide layer spalls after the third cycle of oxidation process.

In the second model, after the first cycle of oxidation process, the oxide layer detached from the matrix and spalled. These models are illustrated in Fig. 17.

Oxidation at the uncoated side took place because of oxygen

Figure 16. Scanning electron micrographs of uncoated side (surface and matrix) after cyclic oxidation showing:
(a) surface oxide layer before spalling.
(b) surface oxide layer after spalling.

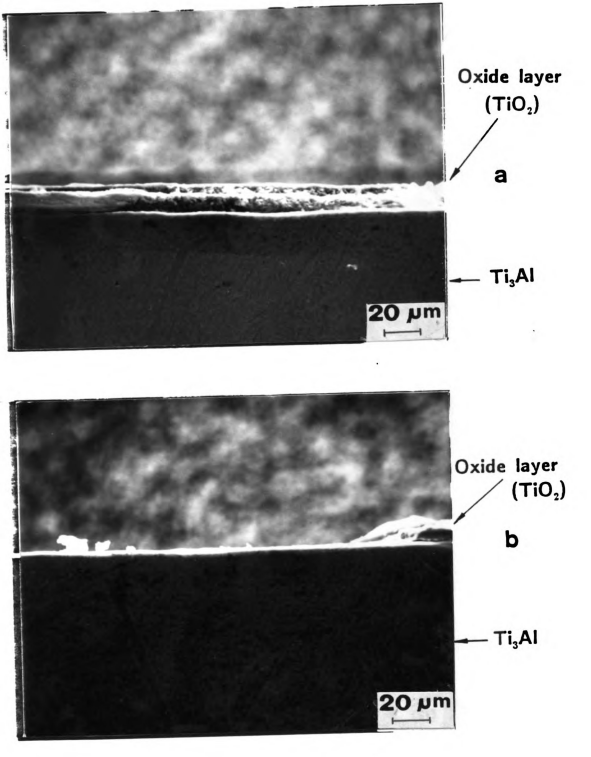

Figure 16.

Figure 17. The schematic diagram of spalling models at the surface of uncoated side during cyclic oxidation process.

(a) The first spalling model.

(b) The second spalling model.

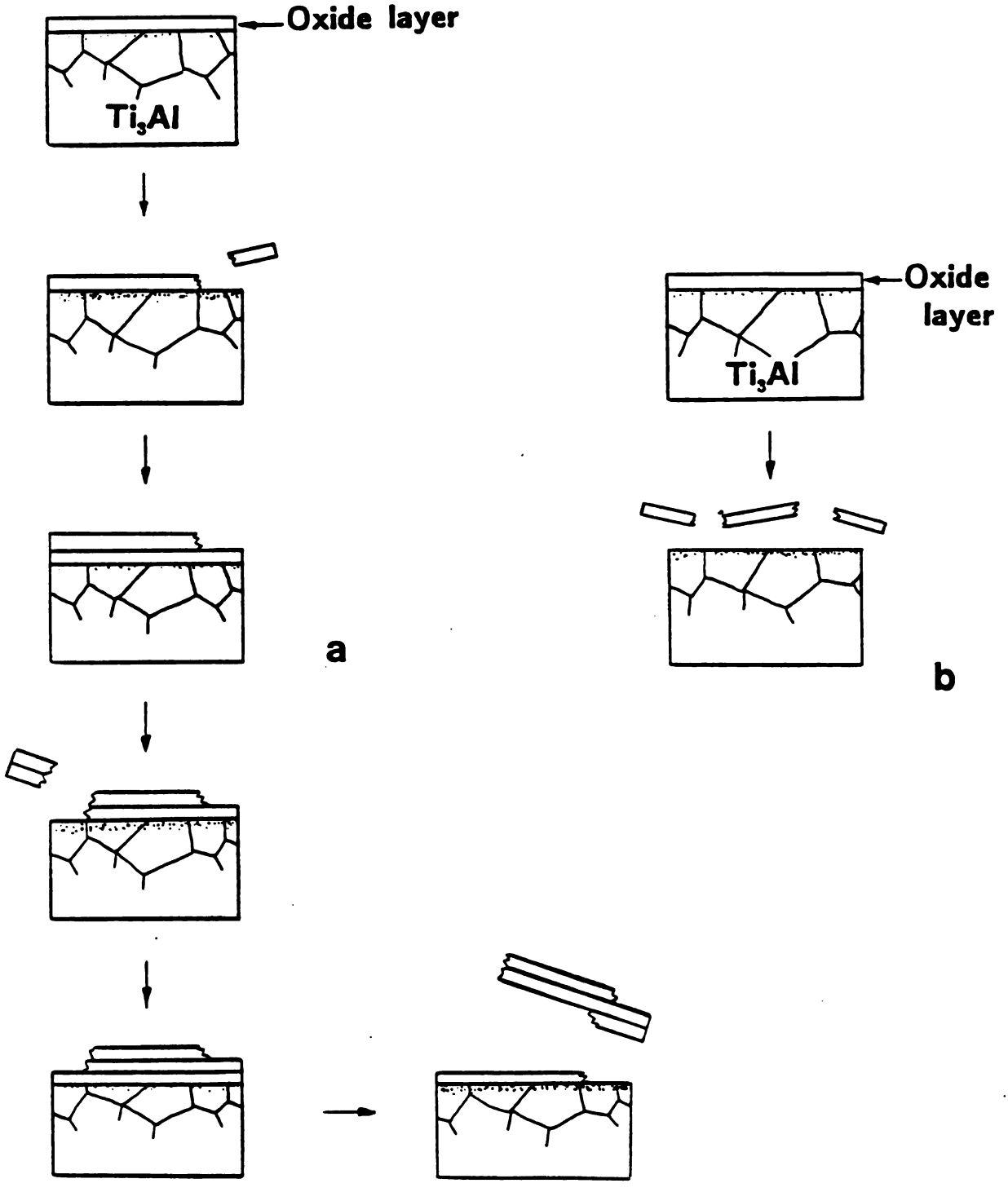

Figure 17.

penetration. The penetration depth of oxygen depends on the oxidation time and temperature [37,42].

The damaged spots at the surface caused by the cutting operation, in spite of being very small, exhibited a larger degree of oxidation as compared to the other regions of the uncoated surfaces (Fig. 18). The damaged spots on the surface could be exposed pores as a result of cutting, or due to cracks between grains. Oxides in the damaged spots did not spall, since they adhered to the small spaces between the grains. Such damaged spots played an important role as the origin of further oxidation of the matrix. (Fig. 19) On the other hand, the oxide layer on the coated side did not spall because the tiny pores in the coating absorbed the stress and strain transmitted from the matrix. The strong adherence (due to diffusion between the oxide layer and the coating) prevented the oxide layer from spalling.

Figure 18. Scanning electron micrograph of the damaged spot at the surface.

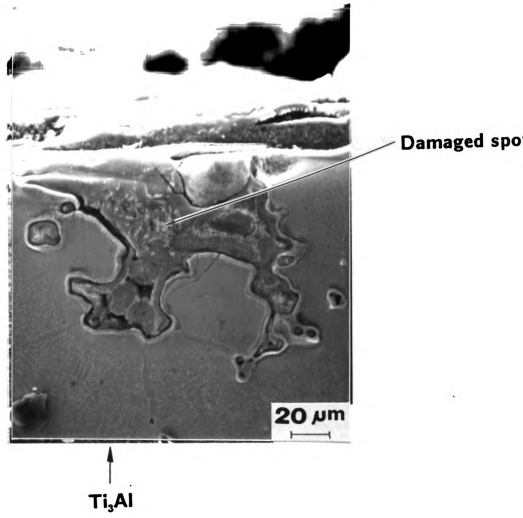

Figure 18.

Figure 19. Scanning electron micrograph of the damaged spot showing further oxidation into the matrix.

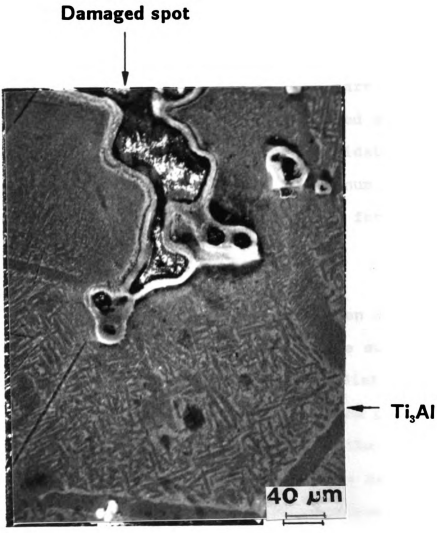

Figure 19.

3-2. CHRACTERISTIC X-RAY STUDY

3-2-1. Characteristic X-ray Image

Characteristic X-ray image studies were carried out on the surface, interface and matrix of the coated and uncoated sides before and after cyclic oxidation process. Concentration profiles of titanium, aluminum, and oxygen were taken from the same regions selected for the SEM studies.

Before the cyclic oxidation process, uneven distributions of titanium and aluminum were observed in the surface of the Al_3Ti coating. A small amount of oxygen distribution was also found here. Such features were caused partly by the laser surface modification and partly by the beginning of the oxide formation. Unfortunatly, it was hard to guess the kind of oxide which was formed at the surface because the concentration profiles of three elements (titanium, aluminum and oxygen) were all mixed up (Fig. 20)

But after the cyclic oxidation process, the oxygen concentration was found to be very high only at the surface, which indicated the presence of an oxide layer at the surface of the Al_3Ti coating. The titanium concentration

Figure 20. Characteristic X-ray image at the surface of the coating after laser suface modification for:
(a) titanium. (b) aluminum.

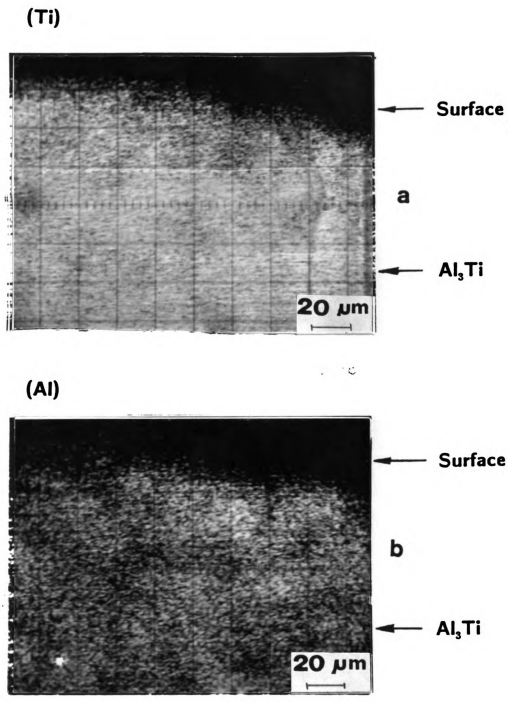

Figure 20.

Figure 20. (continued)
Characteristic X-ray image at the surface of the coating after laser suface modification for:
(c) oxygen.

(Oxygen)

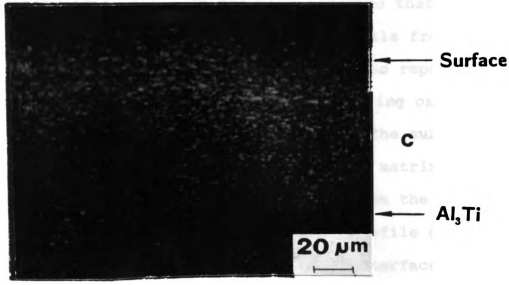

Figure 20. (continued)

profile was uniform throughout the specimen except in the oxide layer on the Al_3Ti coating. The concentration of titanium at the oxide layer was negligible. On the other hand, the aluminum concentration in the oxide layer on the Al_3Ti coating was much higher than that in other regions of the specimen. These results indicated that the oxide layer was composed of alumina. Alumina was formed on the surface of the coating because of higher aluminum contents in the Al_3Ti coating (Fig. 21). It has been reported that the higher aluminum protects this type of materials from oxidation [24]. Subrahmanyam et al. [45] also reported that Al_3Ti was more effective than TiAl in preventing oxygen penetration. Oxygen was not detected below the surface oxide layer (viz. the coating, interface and matrix) because the oxide layer protected the coated side from the oxidation. A change in the concentration profile of titanium and aluminum was observed at the interface between the coating and the matrix. Titanium concentration increased and aluminum concentration decreased below the interface because Al_3Ti was coated on the Ti_3Al (Fig. 22)

On the uncoated side, three kinds of oxygen concentration profiles were detected. The first profile was matched to the scanning electron micrographs obtained from the surface of uncoated side which had several oxide layers.

Figure 21. Characteristic X-ray image at the surfce of the coating after cyclic oxidation process for:
(a) titanium. (b) aluminum.

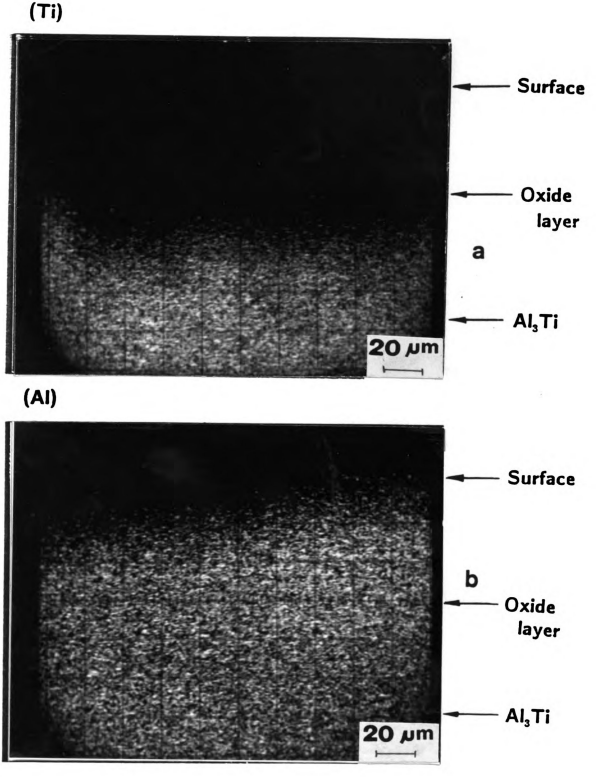
(Ti)
Surface
Oxide layer
a
Al_3Ti
20 μm
(Al)
Surface
b
Oxide layer
Al_3Ti
20 μm

Figure 21.

Figure 21. (continued)
Characteristic X-ray image at the surfce of the coating after cyclic oxidation process for:
(c) oxygen.

(Oxygen)

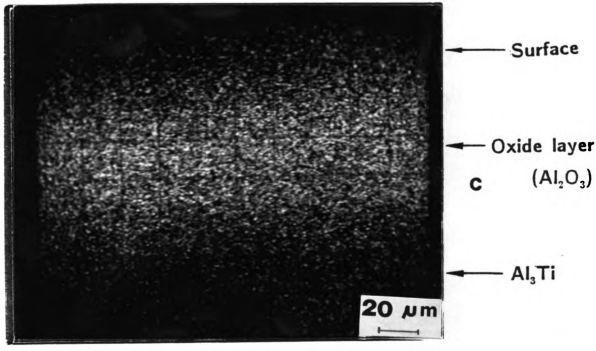

Figure 21. (continued)

Figure 22. Characteristic X-ray image at the interface of the coating after cyclic oxidation process for:
(a) titanium. (b) aluminum.

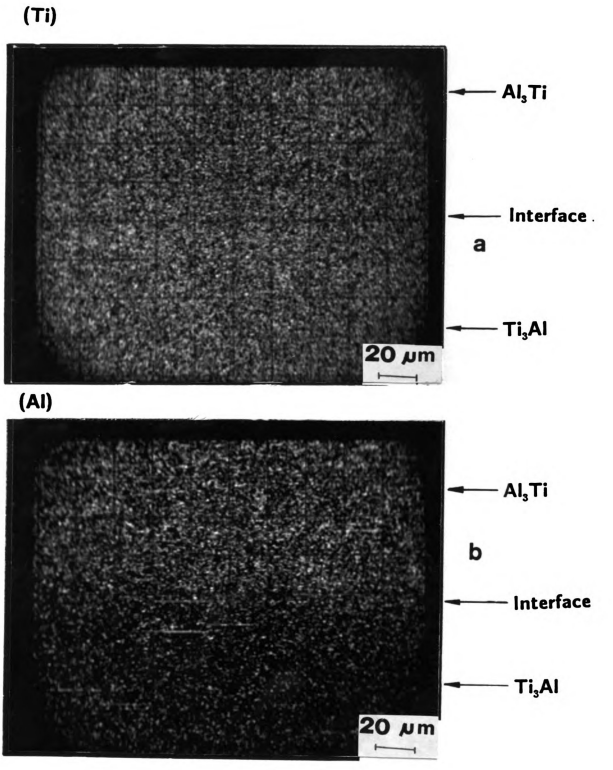
(Ti)
Al_3Ti
Interface
a
Ti_3Al
20 μm
(Al)
Al_3Ti
b
Interface
Ti_3Al
20 μm

Figure 22.

Figure 22. (continued)
Characteristic X-ray image at the interface of the coating after cyclic oxidation process for:
(c) oxygen.

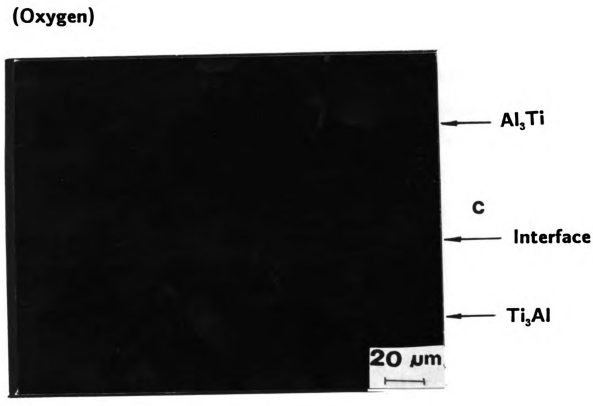

Figure 22. (continued)

The second profile was for the uncoated surface in which fully developed oxide layers had already spalled off and the the oxide layer developed during initial stage was left on the top of the surface. Insignificant oxygen concentration was detected in this region (Fig. 23). The oxygen level of the damaged spot was much higher than that of the others (Fig. 24). Trapped pores (which were also damaged spots) in the matrix had a slightly higher oxygen level than that of matrix because they had trapped oxygen within them (Fig.25). The oxidation process also had occurred inside the wall of pores. All the above results matched the results of the SEM studies.

Figure 23. Characteristic X-ray image at the surface of the uncoated side after cyclic oxidation process for oxygen:
(a) before spalling. (b) after spalling.

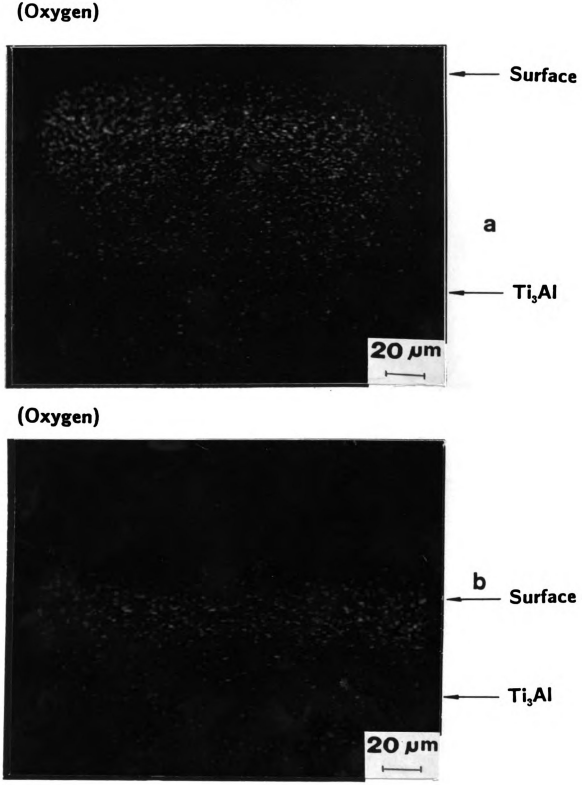

Figure 23.

Figure 24. Characteristic X-ray image at the damaged spot.

(Oxygen)

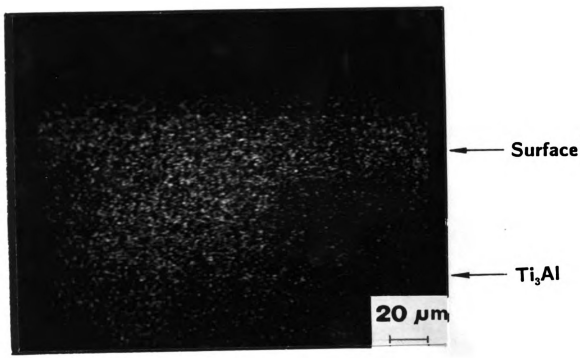

Figure 24.

Figure 25. (a) Characteristic X-ray image at the trapped pore for oxygen and (b) corresponding scanning electron micrograph.

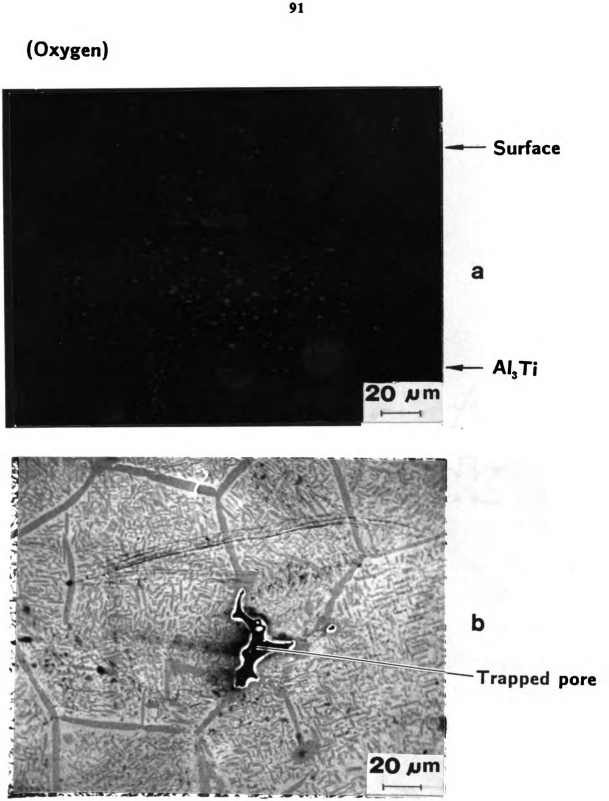

Figure 25.

3-2-2. Line Scanning

Line scanning was carried out on the same areas as those selected for SEM and characteristic X-ray image studies. A scan line consisting of a set of successive points was chosen along the specimen surface. Line scanning could not describe the overall concentration profile of the elements as the area (image) scanning did, but was useful in describing the change of concentration along a line. The line scans for titanium, aluminum and oxygen were carried out before and after the cyclic oxidation process.

Before the cyclic oxidation process, the concentration level for titanium and aluminum was not uniform in the coating but was uniform in the matrix. It was also observed that the scans for the titanium and aluminum concentrations changed sharply at the interface. Only one high peak for oxygen was obtained in the full scanned line, which proved that the oxide layer was already formed on the surface of the Al_3Ti coating after laser surface modification. Other than that peak, no other oxygen peaks were detected in the coating, interface and matrix (Fig. 26).

Figure 26. Characteristic X-ray line scanning before cyclic oxidation process at the coated side showing concentration profiles for:
(a) titanium.

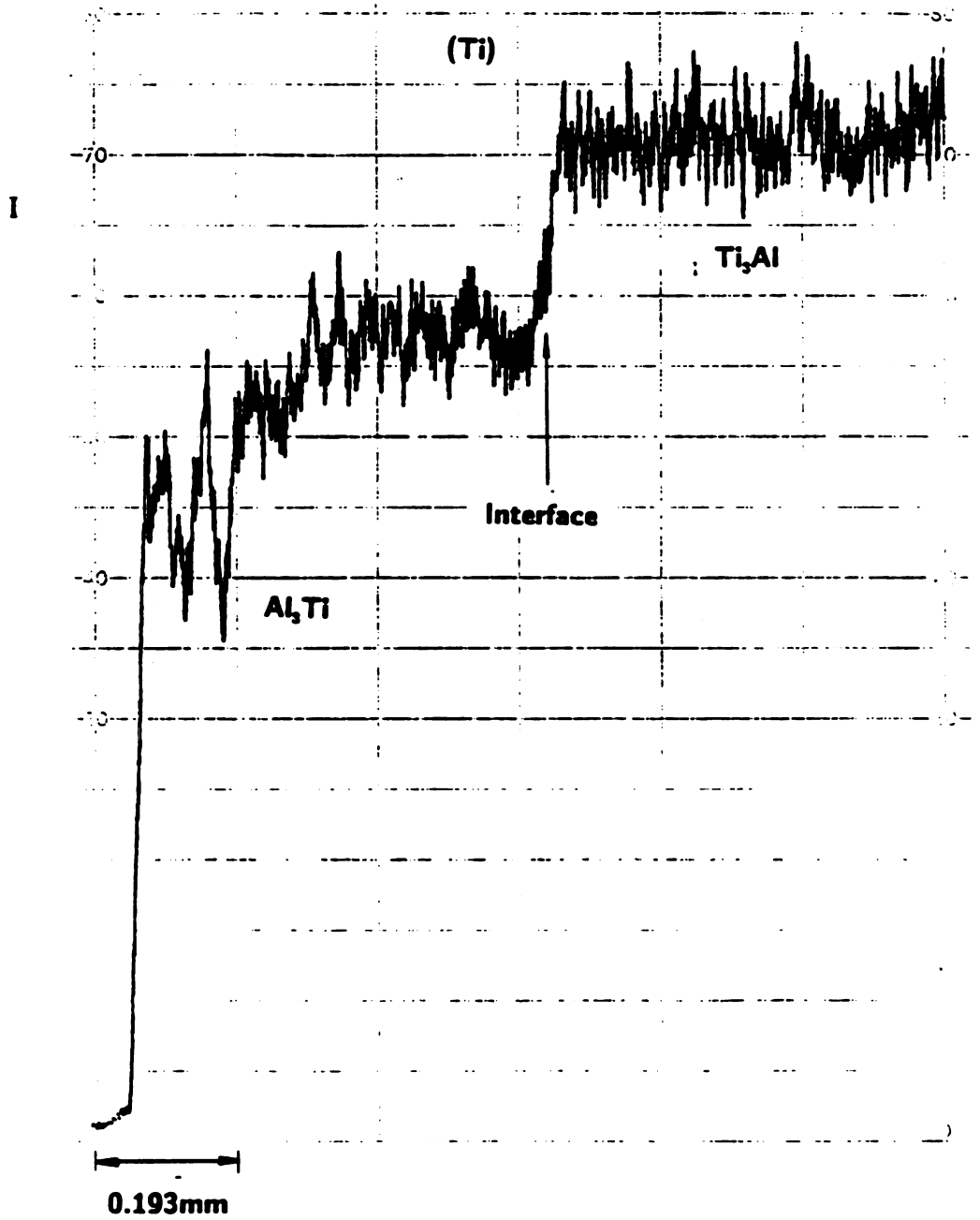

Figure 26.

Figure 26. (continued)
Characteristic X-ray line scanning before cyclic oxidation process at the coated side showing concentration profiles for:
(b) aluminum.

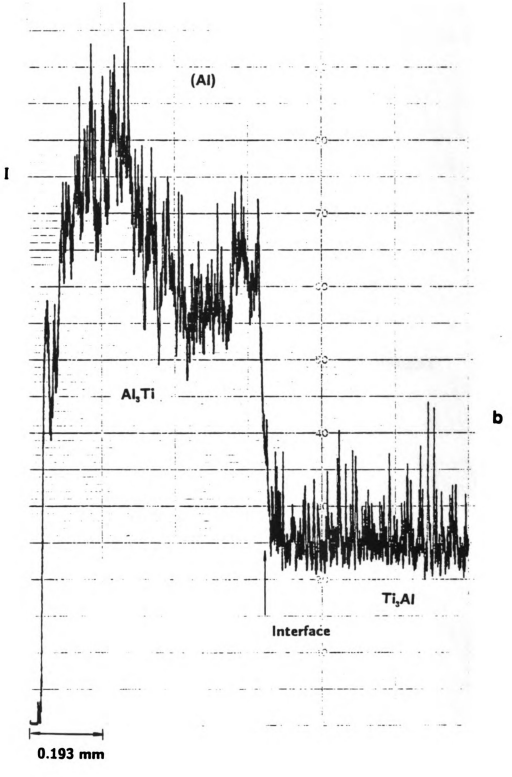

Figure 26. (continued)

Figure 26. (continued)
Characteristic X-ray line scanning before cyclic oxidation process at the coated side showing concentration profiles for:
(c) oxygen.

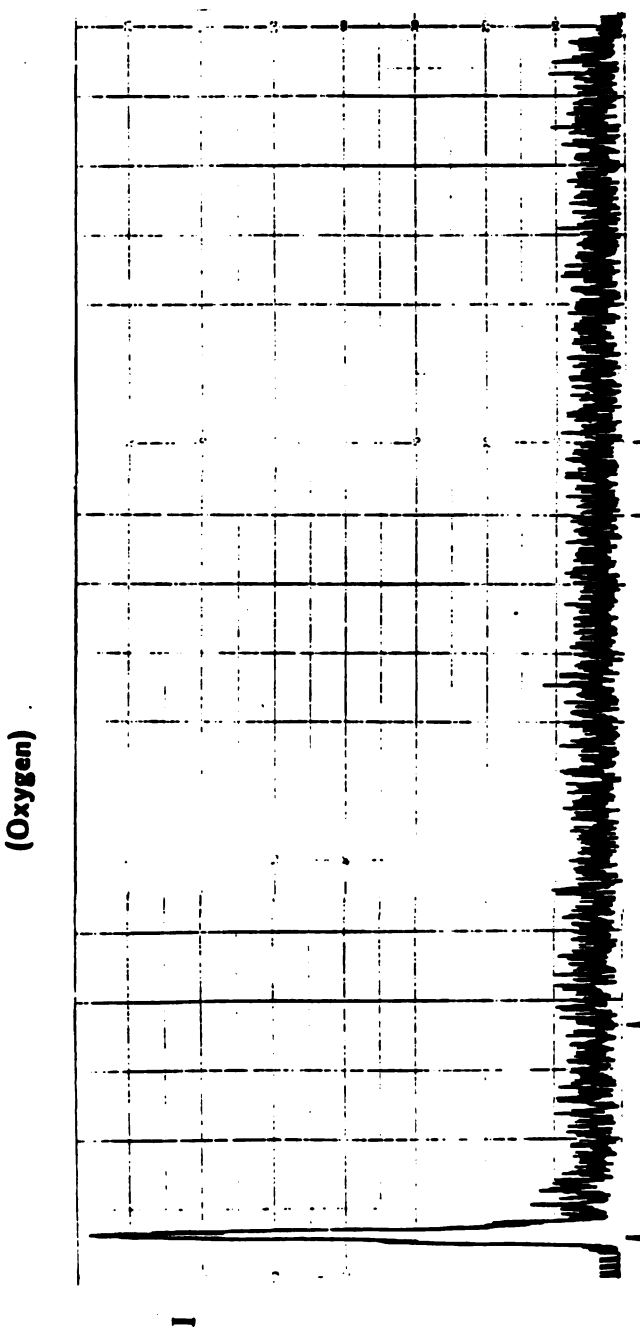

Figure 26. (continued)

After 10 hours of cyclic oxidation process, the concentration levels of titanium and aluminum in the coating became more uniform like those in the matrix because of diffusion. During the oxidation process, some amount of titanium in the matrix diffused to the coating and some amount of aluminum in the coating diffused in the direction opposite to that of the titanium flow. Hence, the concentration profiles of titanium and aluminum, more or less, smoothened at the interface, and the coating grew thicker than before. The concentration profile of oxygen was almost the same as that before cyclic oxidation except for differences in the peak width of the oxide layer. The peak in the oxygen scan increased in width slightly because of the growth of oxide layer during the cyclic oxidation process. Besides this peak, no other peaks were observed throughout the specimen (Fig. 27). This also proved that the coated side (coating, interface and matrix) was protected well from the oxidation even after the cyclic oxidation process.

On the other hand, several oxygen peaks were seen at or near the surface of the uncoated side. The size of the oxygen peaks at the surface were largest, and were followed by smaller ones in the decreasing order of oxygen concentrations (Fig. 28). Peaks which did not follow this

Figure 27. Characteristic X-ray line scanning after cyclic oxidation process at the coated side showing concentration profiles for:
(a) titanium.

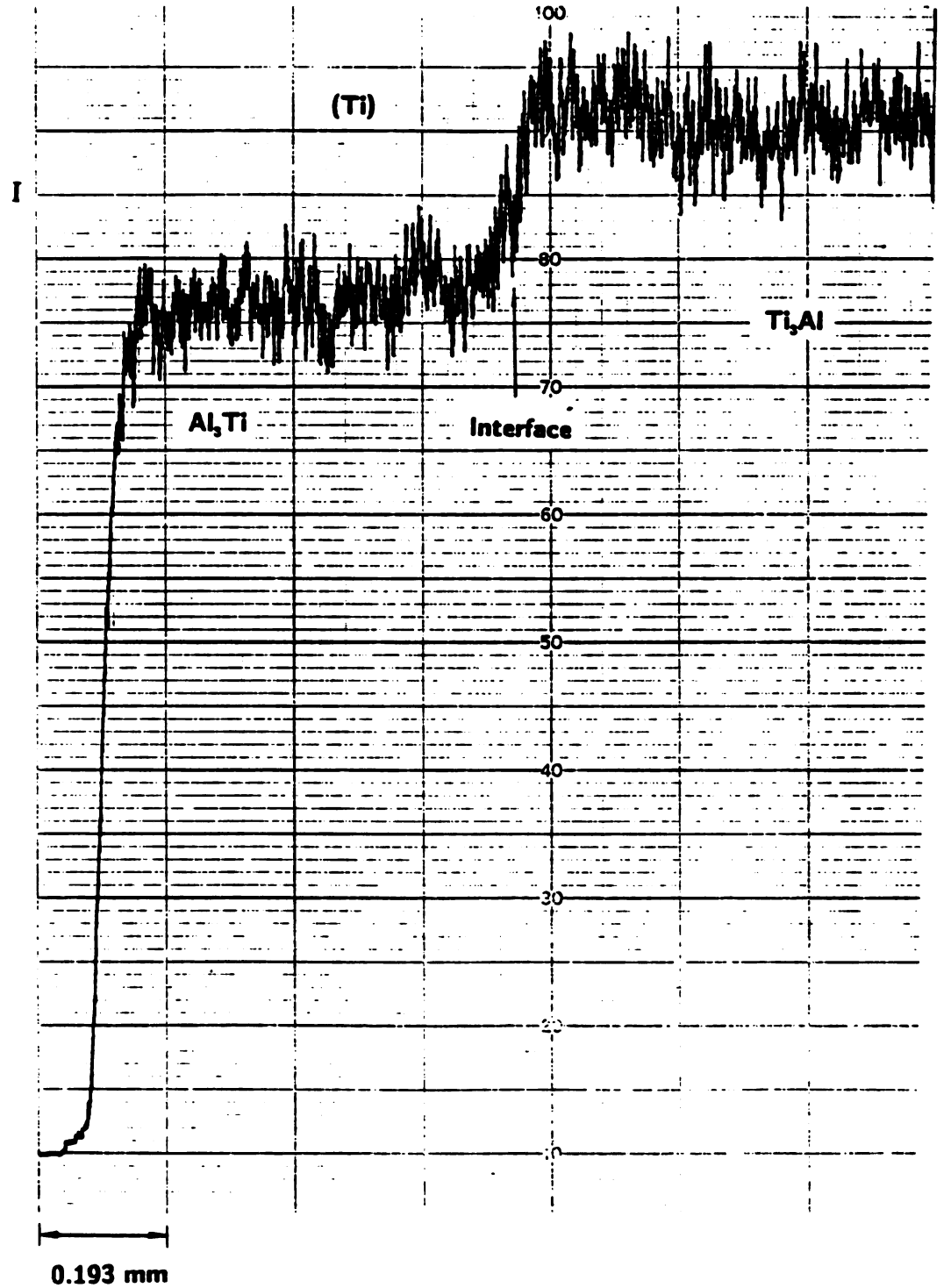

Figure 27.

Figure 27. (continued)
Characteristic X-ray line scanning after cyclic oxidation process at the coated side showing concentration profiles for:
(b) aluminum.

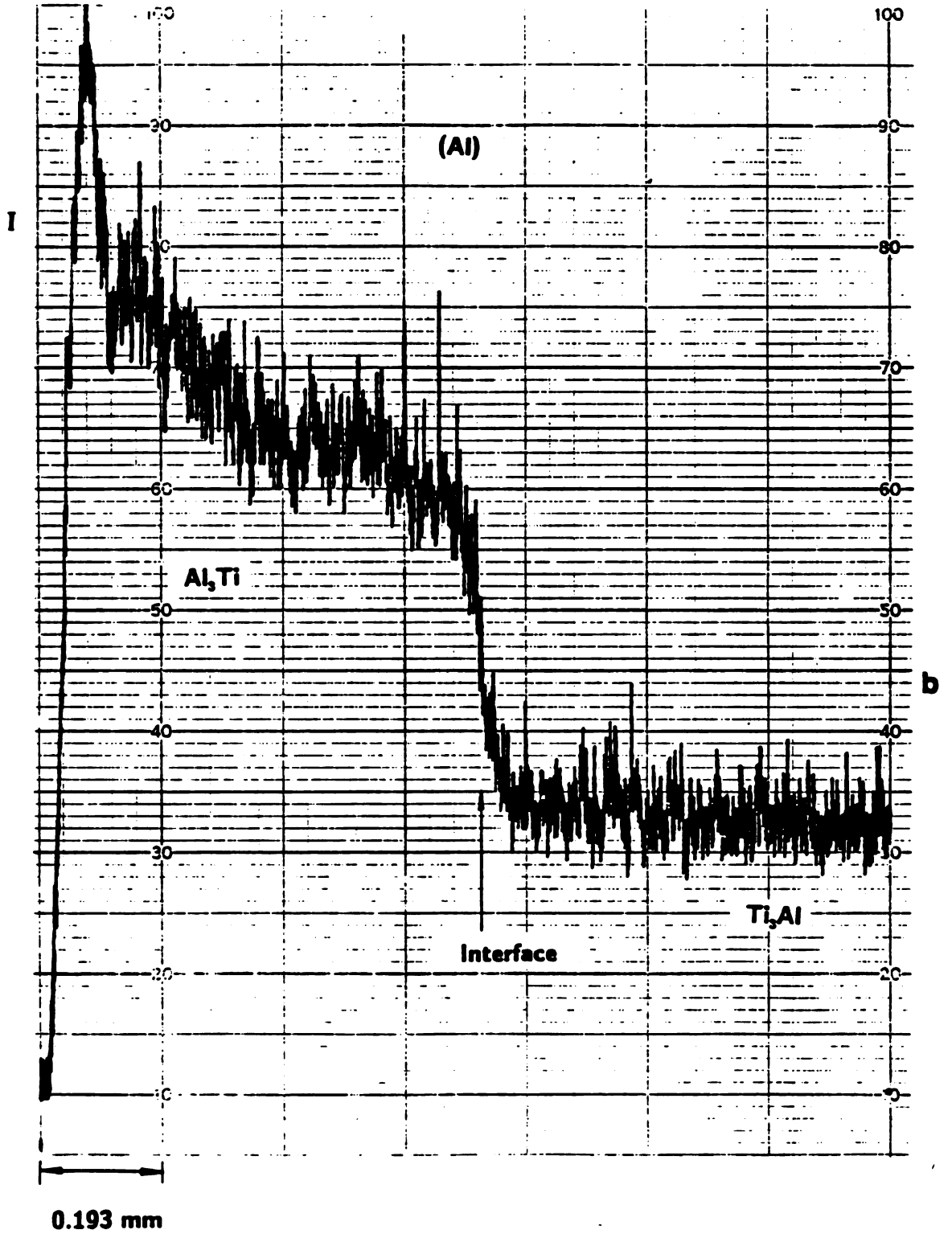

Figure 27. (continued)

Figure 27. (continued)
Characteristic X-ray line scanning after cyclic oxidation process at the coated side showing concentration profiles for:
(c) oxygen.

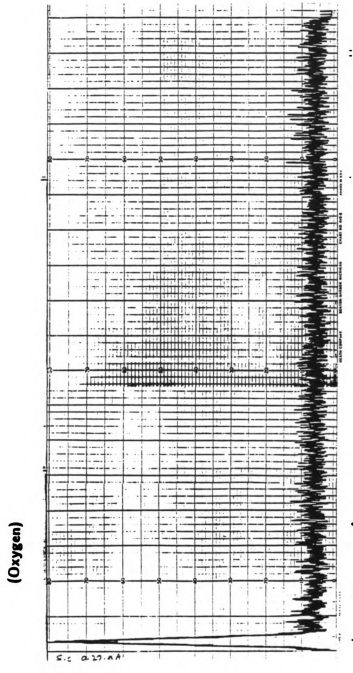

Figure 27. (continued)

Figure 28. (a) Oxygen concentration profiles at uncoated sides after cyclic oxidation process.

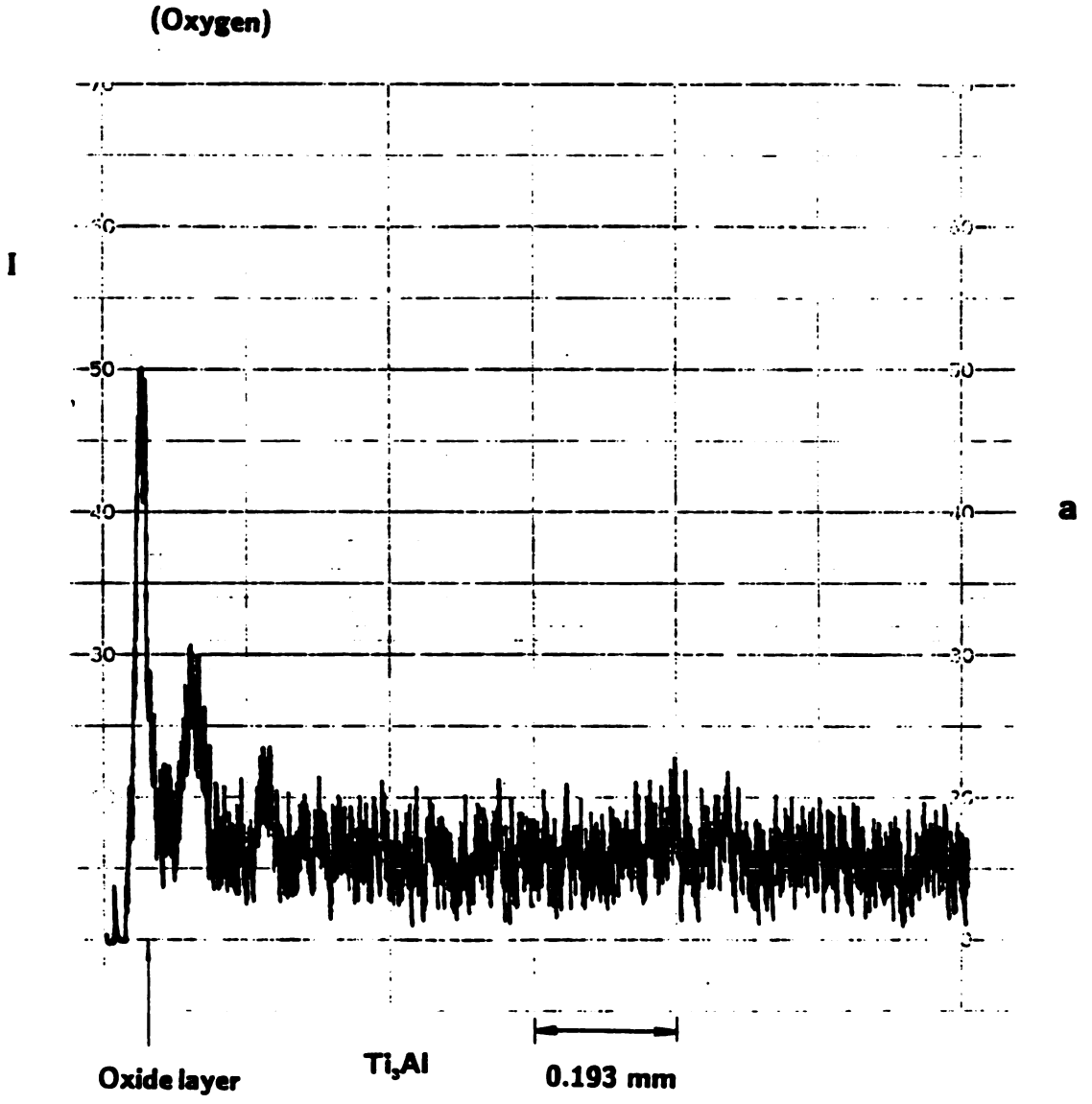

Figure 28.

Figure 28. (continued)

(b) Oxygen concentration profiles at uncoated sides after cyclic oxidation process.

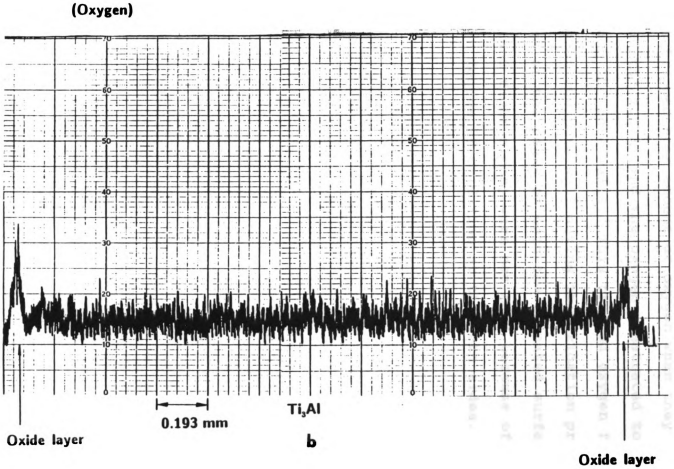

Figure 28. (continued)

trend were detected in the middle of the full scan line because of the presence of trapped pores (Fig.29). Pores trapped some amount of oxygen when they were formed inside the matrix and the oxygen penetrated to the matrix through the pore walls. This trapped oxygen formed the oxide on the pore wall during the oxidation process. The shapes of the peaks on both the uncoated surfaces (on the left and right sides) were not same because of differences in the degree of oxidation at the both sides.

Figure 29. (a) Oxygen concentration profiles at uncoated sides after cyclic oxidation process showing trapped pores.

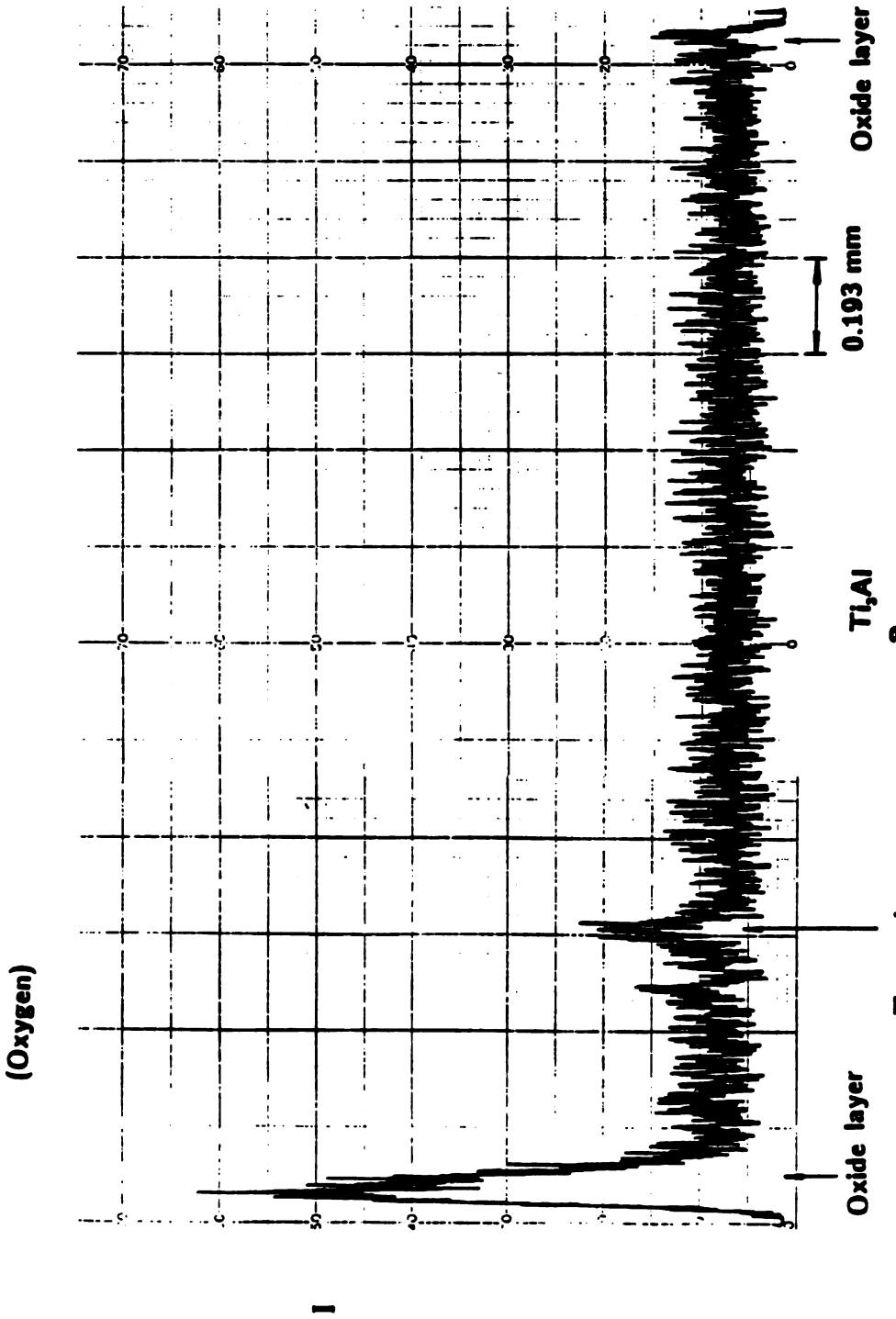

Figure 29.

Figure 29. (continued)

(b) Oxygen concentration profiles at uncoated sides after cyclic oxidation process showing trapped pores.

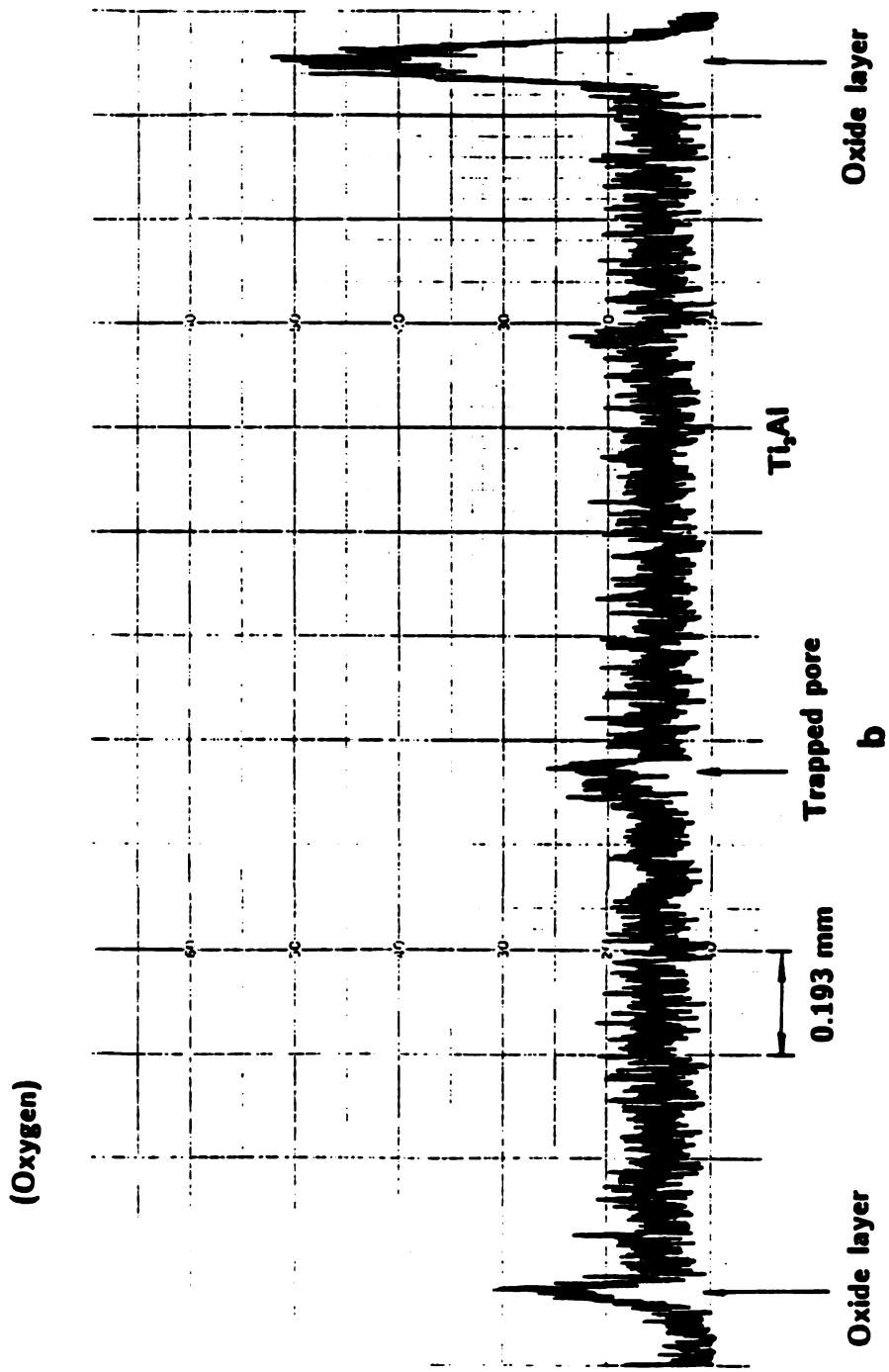

Figure 29. (continued)

4. CONCLUSIONS

1. Al_3Ti coating was formed on the Ti_3Al substrate by using the method of laser surface modification. This process used in the present study is simple, convenient, effective and satisfactory.

2. After laser surface modification process, the oxide layer formed on the surface of the Al_3Ti coating protected the Ti_3Al substrate as well as the coating itself from the oxidation during the 10 hours cyclic oxidation process (1 hour of oxidation at 1000°C and 15 minutes cooling at ambient temperature during each cycle).

3. The oxide layer formed on the surface of the uncoated Ti_3Al substrate spalled off after every cycle of cyclic oxidation process. This was caused by the stress and strain transmitted from the substrate and by the stress and strain which occured in the oxide layer during the cyclic oxidation process.

4. The oxide layer formed on the coated side was Al_2O_3 and that formed on the uncoated side was TiO_2.

5. The strain and stress caused by thermal expansion mismatch between the coating and the substrate did not cause the surface oxide layer on the Al_3Ti coating spall off during the 10 hours cyclic oxidation process.

6. The interface between the Al_3Ti coating and Ti_3Al substrate moved down slightly to the substrate side during the oxidation process due to interlayer diffusion.

REFERENCES

1. F.H. Froes, "The Advanced Aerospace Structural Materials Dilemma", J. Metals, pp 30-35 (1989)

2. J. Wadsworth and F.H. Froes, "Developments in Metallic Materials for Aerospace Applications", J. Metals, pp 12-19 (1989)

3. P. Cannon, "Aerospace Materials for the 21st Centuries", J. Metals, pp 11-14 (1988)

4. M.B. Bever, ed. Encyclopedia of Materials Science and Engineering, 4, pp 2502-2505, Pergamon Press Oxford (1986)

5. Y.W. Kim, "Intermetallic Alloys Based on Gamma Titanium Aluminide", J. Metals, pp 24-30 (1989)

6. M.G. Mendiratta and H.A. Lipsitt, " Steady-state creep behavior of Ti-3Al-base intermetallics", J. Material Science, 15, pp 2985-2990(1980)

7. P.L. Martin, Madan G. Mendiratta and H.A. Lipsitt, "Creep Deformation of TiAl and TiAl+W Alloys", Metallurgical Transactions A, 14A, pp 2170-2174 (1983)

8. S.H. Whang and Z.X. Li, "Tetragonal Distortion and its Relaxation in Rapidly Quenched L1o TiAl Compounds", Material Science and Engineering, 98, pp 269-272 (1988)

9. S.R. Schuon and A.P. Druschitz, " Microalloying TiAl with Nitrogen and Tungsten", J. Metals, pp 36-37 (1987)

10. R.L. Fleischer and A.I. Taub, " Selecting High-Temperature Structural Intermetallic Compounds: The Materials Science Approach," J. Metals, pp 8-11 (1989)

11. F.H. Froes, "Structural Intermetallics", J. Metals, pp 6-7 (1989)

12. C. Bassi, J.A. Peters and J. Wittennauer, "Processing Titanium Aluminide Foils", J. Metals, pp 18-20 (1989)

13. H.A. Lipsitt, D. Shechtman, and R.E. Shafrik, "The Deformation and Fracture of Tl_3Al at Elevated Temperatures", Metallurgical Transactions A, 11A, pp 1369-1375 (1980)

14. J.A. Graves, L.A. Bendersky and F.S. Biancaniello, J.H. Perepezko and W.J. Boettinger, "Pathways for Microstructural Development in TiAl", Materials Science and Engineering, 98, pp 265-268 (1988)

15. M.J. Kaufman, D.G. Konitzer, R.D. Shull and H.L. Fraser, "An Analytical Electron Microcopy Study of the recently Reported Ti_2Al Phase in -TiAl Alloys", Scripta Metallurgica, 20, pp 103-108 (1986)

16. H.A. Lipsitt, D. Shechtman, and R.S. Shafrik, "The Deformation of Fracture of TiAl at Elevated Temperatures", Metallurgical Transactions A, 6A, pp 1991-1996 (1975)

17. D. Sechtman, M.J. Blackburn and H.A. Lipsitt, "The Plastic Deformation of TiAl", Metallurgical Transactions, 5, pp 1373-1381 (1974)

18. R.E. Schafrik, "Dynamic Elastic Moduli of the Titanium Aluminides", Metallurgical Transactions A, 8A, pp 1003-1007 (1977)

19. R.J. Kerans, "Deformation in Ti_3Al Fatigued at Room and Elevated Temperatures", Metallurgical transactions A, 15A, pp 1721-1729 (1984)

20. T. Takemoto and I. Okamoto, "Intermetallic compounds formed during brazing of titanium with aluminium filler metals", J. Material Science, 23, pp 1301-1308 (1988)

21. J. Holwach and T. Redden, "Ti/Al design/cost trade-off analysis", AFAPL-TR-78-74 (General Electric Co., Cincinati, Ohio, 1978)

22. M.G. Mendiratta and N.S. Chowdary, "Properties and report, AFML-TR-78-112 (Systems Research Laboratories Inc., Dayton, Ohio, 1978)

23. C.T. Sims, N.S. Stoloff, W.C. Hagel, Super Alloys II, pp 519-558, John Wiley & Sons (1987)

24. M. Yamaguchi, Y. Umakoshi and T. Yamane, "Deformation of the Intermetallic Compound Al_3Ti and Some Alloys with an Al_3Ti Base", MRS Symposium Proceeding, 81, pp 275-285 (1987)

25. H.A. Lipsitt, "Titanium Aluminudes-An Overview", MRS Symposium Proceedings, 39, pp 351-364 (1985)

26. D.A. Porter and K.E. Easterling, Phase Transformations in Metals and Alloys, pp 1-446, Van Nostrans Reinhold Co., New York (1981)

27. P.C. Gehlen, "The Lattice Parameters of Ordered Ti_3Al between 100 and 989°K", Metallurgical Transactions, 2, pp 1259-1251 (1971)

28. T. Kawabata and O. Izumi, "Dislocation Reactions and Fracture Mechanism in TiAl L1o Type Intermetallic Compound", Scripta Metallurgica, 21, pp 435-440 (1987)

29. D.L. Anton, D.M. Shah, D.N. Duhl and A.F. Giamei, "Selecting High-Temperature Structural Intermetallic Compounds:The Engineering Apporach", J. Metals, pp 12-17 (1989)

30. J. Doychak and T. Grobstein, "The Oxidation of High Temperature Intermetallics", J. Metals, pp 30-31 (1989)

31. J. Tarnacki and Y.W. Kim, " A Study of Rapidly Solidified Al_3Ti Intermetallics with Alloying Additions." Scripta Metallurgica, 22, pp 329-334 (1988)

32. R.A. Perkins, K.T. Chiang and G.H. Meier, "Formation of Alumina on Ti-Al Alloys", Scripta Metallurgica, 21, pp 1501-1510 (1987)

33. N.S. Stoloff, "Ordered Alloys for High Temperature Applications", MRS Sysmposium Proceedings, 39, pp 3-27 (1985)

34. J. Subrahmanyam, "Cyclic oxidation of aluminized Ti-14Al-24Nb alloy," J. Material Science, 23, pp 1906-1910 (1988)

35. C.A. Barrett and C.E. Lowell, "High Temperature Cyclic Oxidation Furnace Testing at NASA Lewis Research Center", JTEVA, 10, No.6, pp 273-278 (1982)

36. A.M. Chaze and C. Coddet, "Influence of Chromium on the Oxidation of Titanium Between 550 and 700°C", Oxidation of Metals, 21, Nos.3/4, pp 205-231 (1984)

37. J.E. Gomes Lopes and A.M. Huntz, "Comparison of the Kinetics and Morphologic Properties of Titanium, Ti-1.5N and Ti-2,5Cu During Oxidation in Pure Oxegen Between 600 and 820°C", Oxidation of Metals, 14, No.6, pp 471-498 (1980)

38. A. Abba, A. Galerie, and M. Caillet, "High-Temperature Oxidation of Titanium Silicide Coatings on Titanium", 17, No.1, pp 43-54 (1982)

39. A. Galerie and G. Dearnaley, "Production of Ti-Si Surface Alloys on Titanium by Ion Beam Mixing, and their Oxidation Behavior", 69, pp 381-390 (1985)

40. A.M. Chaze and C. Coddet, "Influence of Silicon on the Oxidation of Titanium between 550 and 700°C", Oxidation of Metals, 27, Nos.1/2, pp 1-20 (1987)

41. J. Unnam, R.N. Shenoy, and R.K. Clark, "Oxidation of Commercial Purity Titanium", Oxidation of Metals, 26, Nos.3/4, pp 231-252 (1986)

42. A.M. Chaze and C. Coddet, "Influence of alloying elements on the dissoution of oxygen in the metallic phase during the oxidation of titanium alloys", J. Material Sceince, 22, pp 1206-1214 (1987)

43. F. Abe, H. Yoshida, and M. Okada, " The Role of Aluminium and Titanium on the Oxidation Process of a Nickel-Base Superalloy in Steam at 800°C", Oxidation of Metals, 27, Nos.1/2, pp 21-36 (1987)

44. R.K. Clark, J. Unnam, and K.E. Wiedemann, "Effect of Coatings on Oxidation of Ti-6Al-2Sn-4Zr-2Mo Foil", Oxidation of Metals, 29, Nos.3/4, pp 255-268 (1988)

45. J. Subrahmanyam and J. Annapurana, "High Temperature Cyclic Oxidation of Aluminude Layers on Titanium", Oxidation of Metals, 26, Nos.3/4, pp 275-285 (1986)

46. S.M.L. Sastry and H.A. Lipsitt, "Cyclic Deformation of Ti_3Al", Acta Metallurgica, 25, pp 1279-1288 (1977)

47. S.C. Jha, T.A. Mozhi and R. Ray, "Rapidly Solidified Ai-Ti Alloys via Advanced Melt Spinning", J. Metals, pp 27-30 (1989)

48. V.G. Gregson, Laser Heat Treatment. pp 203-233, North-Holland Publishing Co. (1983)

49. H.W. Bergman, "Laser Surface Melting of Iron-Base Alloys", NATO ASI Series, pp 351-367 (1986)

50. Y. Nilsson, " Surface Melting of Cast Iron with a High Power Beam", MRS Symposium Proceedings, 8, pp 517-521 (1982)

51. T. Chande and J. Mazumder, "Dimensionless parameters for process control in laser surface alloying", Optical Engineering, 22, No.3, pp 362-365 (1983)

52. J. Mazumder, Laser Welding, pp 115-200, North-Holland Publishing Co. (1983)

53. J. Mazumder and J. Singh, "Laser Surface Alloying and Caldding for Corrosion and Wear", NATO ASI Series, pp 297-307 (1986)

54. C. Marsden, D.R.F. West, and W.M. Steen, "Laser Surface Alloying of Stainless Steel with Carbo", NATO ASI Series, pp 461-473 (1986)

55. B.R. Mordike and H.W. Bergman, "Surface Alloying of Iron Alloys by Laser Beam Melting," MRS Symposium Proceedings, 8, pp 463-477 (1982)

56. J.T. Luxon, D.E. Parker and P.D. Plotkowski, Lasers in Manufacturing, pp 53-62, IFS Ltd, (1987)

57. P.J.Okley and N.bailey, "Laser surface of nickel aluminium bronze", Laser welding, machining and materials processing, Laser Institute of America, pp 169-177 (1986)

58. F.J.J. van Loo and G.D. Rieck, "Diffusion in the Titanium-Aluminium System-II, Interdiffusion in the Composition Range Between 25 and 100 at % Ti", Acta Metallurgica, 21, pp 73-84 (1973)

59. N. Birks and G.H. Meier, Introduction to High Temperature Oxidation of Metals, pp 1-198, Edward Arnold, (1987)

60. J.K. Tien and J.M. Davison, "Oxide Spallation Mechanisms in Stress Effects and the Oxidation of Metals", edited by J.V. Cathcart, pp 200-219 (1974)

61. M.Schutze, "The limits to the protective effect of oxide scales on high temperature materials which are subhected to strains", High Temperature Alloys, edited by J.B. Marriott, M.Merze, J.Nihoul and J.Ward, Elsevier Applied Science, (1987)